Estuaries and Coasts
DOI 10.1007/s12237-009-9202-8

Peat Accretion Histories During the Past 6,000 Years in Marshes of the Sacramento–San Joaquin Delta, CA, USA

Judith Z. Drexler · Christian S. de Fontaine · Thomas A. Brown

Received: 14 January 2009 / Revised: 16 June 2009 / Accepted: 7 July 2009

Abstract The purpose of this study was to determine how vertical accretion rates in marshes vary through the millennia. Peat cores were collected in remnant and drained marshes in the Sacramento–San Joaquin Delta of California. Cubic smooth spline regression models were used to construct age–depth models and accretion histories for three remnant marshes. Estimated vertical accretion rates at these sites range from 0.03 to 0.49 cm year^{-1}. The mean contribution of organic matter to soil volume at the remnant marsh sites is generally stable (4.73% to 6.94%), whereas the mean contribution of inorganic matter to soil volume has greater temporal variability (1.40% to 7.92%). The hydrogeomorphic position of each marsh largely determines the inorganic content of peat. Currently, the remnant marshes are keeping pace with sea level rise, but this balance may shift for at least one of the sites under future sea level rise scenarios.

Keywords Autocompaction · Radiocarbon age determination · Sea level rise · Soil volume · Tidal freshwater marsh · Vertical accretion

J. Z. Drexler (✉) · C. S. de Fontaine
US Geological Survey, California Water Science Center,
6000 J Street, Placer Hall,
Sacramento, CA 95819-6129, USA
e-mail: jdrexler@usgs.gov

T. A. Brown
Center for Accelerator Mass Spectrometry,
Lawrence Livermore National Laboratory L-397,
P.O. Box 808, 7000 East Avenue,
Livermore, CA 94551, USA
e-mail: tabrown@llnl.gov

Introduction

Marshes form where hydrologic, geomorphic, and ecologic factors are conducive to the initial and continued accretion of mineral sediment and organic matter (OM; Anisfield et al. 1999; Reed 2000). In tidal freshwater marshes, such accretion ultimately leads to the formation of peat soils. The rate at which peat vertically accretes varies both spatially and temporally. Spatial variability in accretion can be attributed to differences in ecological factors (e.g., plant community composition, plant productivity, and decomposition rates) and/or physical factors (e.g., tidal amplitude, duration of flooding, proximity to tidal creeks, and sediment load of channels; Khan and Brush 1994; Hensel et al. 1998; Allen 2000; Merrill and Cornwell 2000; Reed 2002a; Temmerman et al. 2003; Schoellhamer et al. 2007; Neubauer 2008). In contrast, temporal variation in accretion rates is largely caused by climatic fluctuations and extreme natural events such as fire and flooding that affect plant productivity and/or sediment supply in channels (Reed 2000; Allen 2000; Wright and Schoellhamer 2005; Schoellhamer et al. 2007). In addition, temporal and spatial changes in vertical accretion can be due to a wide range of human activities including land clearing for agriculture, hydraulic mining for ore, and dam building (Gilbert 1917; Orson et al. 1990; Wright and Schoellhamer 2005).

To date, most marsh studies incorporating temporal variability of accretion rates have focused on short timescales of <10 years up to 100 years. These short-term accretion rates have been compared to current and predicted future rates of sea level rise in order to assess the overall sustainability of coastal marshes (e.g., Stevenson et al. 1986; Penland and Ramsey 1990; Roman et al. 1997; Reed 2002a; Cahoon et al. 2006). Such studies clearly provide insights into the future behavior of marshes. However, due

Published online: 30 July 2009

to their short timescales, they cannot adequately portray the *range* of accretion rates that are feasible in particular marsh settings. For this reason, studies are also needed that estimate accretion processes over timescales that approach or incorporate the entire lifetime of a marsh. Knowledge of long-term rates (millennial scale) can provide a broader context for understanding the intrinsic capability of marshes to continue providing crucial ecosystem services under scenarios of global climate change and associated sea level rise.

Long-term accretion rates in peat are typically estimated using radiocarbon age determination over the entire length of the peat column. Age–depth models are then used to interpolate between dated sections of the peat core. Research has shown, however, that the success of this approach relies heavily on avoiding numerous methodological pitfalls and accounting for all possible error. For example, small depth intervals must be used between radiocarbon samples because larger intervals have been associated with dubious chronologies and highly varying accretion rates (Liu et al. 1992; Reed 2002a). In addition, plant macrofossils must be used for radiocarbon analysis and not bulk peat because bulk peat consists largely of roots which are significantly younger than the actual surface of interest (Kaye and Barghoorn 1964; Tornqvist et al. 1992; van Heteren and van de Plassche 1997). Furthermore, all error related to choosing and analyzing a particular radiocarbon sample and using it to represent a particular depth interval needs to be incorporated into an age–depth model in order to provide realistic error estimates (Heegaard et al. 2005). Peat cores also need to be evaluated for the possibility of autocompaction, which involves settling of inorganic and organic fractions as well as loss of interstitial water in the saturated zone (Kaye and Barghoorn 1964). Approaches exist that can estimate autocompaction and these need to be explored if a significant relationship is found between depth and accretion rate (Kaye and Barghoorn 1964; Stevenson et al. 1986; Pizzuto and Schwendt 1997; Allen 2000). Lastly, for peat-forming regions that are known to be tectonically active, an evaluation of the prospects of subsidence or uplift is essential for proper interpretation of the peat record (e.g., Atwater et al. 1977; Sawai et al. 2002; Tornqvist et al. 2004, 2006).

The Sacramento–San Joaquin Delta (hereafter, the Delta) of California contains a long continuous peat record, making it well suited for studying peat accretion through the millennia. The Delta region, which constitutes the landward limit of the San Francisco Bay Estuary, was once a 1,400-km^2 tidal marsh region that began forming ~6,700 calibrated years before present (cal year BP; Drexler et al. 2007). Between the 1860s and 1930s, the Delta was greatly transformed by drainage and extensive levee building into an agricultural landscape with about 57 farmed islands and tracts (Thompson 1957; Ingebritsen and Ikehara 1999). Such major changes in land use have resulted in land surface subsidence of up to 8 m below sea level, due mainly to microbial oxidation of peat soils (Deverel and Rojstaczer 1996; Deverel et al. 1998; Drexler et al. 2009). The Delta ecosystem has also been strongly impacted by its use as a major water conveyance system for California via the State Water Project and the Federal Central Valley Project. Due to a number of factors including altered flows from massive pumps and management of salinity within a narrow range, several fish species are currently threatened or endangered (Service 2007). Currently, state and federal agencies are working to restore the general ecological health of the region. Wetland restoration has been one of the tools used to increase habitat for sensitive species and improve the general ecological health in the region (Reed 2002b). In addition, wetland restoration has the potential to mitigate land surface subsidence by rebuilding peat (e.g., Miller et al. 1997) and, in so doing, provide the much-needed ecosystem service of sequestering carbon.

In order for wetland restoration to have the best chance of success, scientists and managers need information on peat accretion processes. Furthermore, quantification of peat accretion rates is necessary in order to understand the vulnerability of marshes to inundation from sea level rise. In the Delta, although there have been studies on peat distribution and peat thickness (Atwater 1980, 1982; Atwater and Belknap 1980), little is currently known about how peat started forming and how quickly it has accreted through time. In a rare paper on the quaternary evolution of the Delta, Shlemon and Begg (1975) determined ten radiocarbon dates at progressively deeper depths along an east–west transect in the Delta. Due to the use of large sampling intervals and bulk peat, the data cannot be used to estimate vertical accretion rates. Nevertheless, these data provide an important baseline of peat age against which to compare subsequent data. Methodological issues also exist for a paper by Atwater et al. (1977), which contains a valuable data set of radiocarbon analyses from salt marshes in south San Francisco Bay, the most seaward part of the San Francisco Bay Estuary. More recently, Goman and Wells (2000) determined vertical accretion rates for two peat cores collected at Browns Island (BRI), one of the sites chosen for this study. They used linear age–depth models and found high variability in accretion with depth (0.05–0.41 cm year^{-1}). Reed (2002b) is the only study to focus on recent accretion rates in the Delta. Over a 2-year period, Reed (2002b) determined that rates of vertical accretion were in excess of 1 cm year^{-1} in restored and references marshes, with highest rates at sites closest to the Sacramento River and lowest rates in interior marsh sites. Clearly, more information is needed on the variability and

characteristics of vertical peat accretion in the Delta through time.

The purpose of this study was to determine how peat accretion rates in marshes vary through the millennia. We chose to study four relatively undisturbed remnant marshes and four drained farmed islands (former marshes) in the Delta. The chief objectives of the study were to answer the following questions: (1) how might peat have initially started forming, (2) how quickly has peat accreted through the millennia, (3) and, given past performance, are the remnant marshes capable of keeping pace with current and predicted future rates of sea level rise?

Study Location

The Delta is located at the confluence of the Sacramento and San Joaquin Rivers and receives runoff from over 40% of the land area of California (California Department of Water Resources 1995; Fig. 1). During the last few hundred years, the Delta has been exclusively a freshwater tidal system; however, current geochemical research suggests that salinity may have been brackish during at least some of its history (Charles Alpers, US Geological Survey, unpublished data). Tides are semidiurnal with normal tidal range of approximately 1 m; however, during floods, the river stage can exceed 2 m (Shlemon and Begg 1975; Atwater 1980). The climate in the Delta is characterized as Mediterranean with cool winters and hot, dry summers (Atwater 1980). Mean annual precipitation is approximately 36 cm, but actual yearly precipitation varies from half to almost four times this amount. Over 80% of precipitation occurs from November through March (Thompson 1957). Beginning in the mid-1800s, the Delta was largely drained for agriculture (Thompson 1957; Atwater 1980), resulting in its current configuration of over 100 islands and tracts surrounded by 2,250 km of man-made levees and 1,130 km of waterways (Prokopovich 1985). Subsequent to drainage, land surface subsidence occurred on the farmed islands. Recent rates of land surface subsidence range from approximately 0.5 to 3.0 cm year^{-1} (Rojstaczer and Deverel 1993, 1995; Deverel and Leighton 2009). Land surface subsidence due to natural gas extraction and groundwater withdrawal is estimated to be approximately 0.508 cm year^{-1} in the north and northeastern parts of the Delta, but this gas field is largely outside the area covered by this study (Rojstaczer et al. 1991). Neotectonic subsidence and uplift of ~0.2 to 0.6 mm year^{-1} are thought to be occurring along the west and east side, respectively, of the Midland Fault, which runs approximately north to south bisecting the Delta at Sherman Island (Weber-Band 1998).

Study sites were chosen to encompass the various geomorphic settings and salinity regimes of the Delta. Sites were chosen along the historic floodplain of the Sacramento River as well as the glacial outwash area along the San Joaquin River. In addition, sites were selected from high-energy environments such as the confluence of the Sacramento and San Joaquin Rivers to more quiescent environments such as distributaries of the San Joaquin River. In total, eight sites were chosen including four remnant, relatively undisturbed marsh islands and four nearby drained farmed islands (Fig. 1). Cropping histories for the farmed islands are available in Drexler et al. (2009). On each of the farmed islands, coring was done both near the levee and near the center of the island because land surface subsidence is known to be significantly greater at the center of the islands (Ingebritsen and Ikehara 1999; Mount and Twiss 2005). Coring on the marsh islands was only done near the island centers. Table 1 contains site names and basic site descriptions, including periods of drainage and levee building for each of the farmed islands.

The remnant marsh islands are much smaller than the farmed islands and, because of that, they were not drained for agriculture. Vegetation on the marsh islands is dominated by emergent macrophytes and shrub–scrub wetland species. On BRI, the most brackish of the study sites, vegetation is dominated by *Schoenoplectus americanus* (American bulrush) and *Distichlis spicata* (salt grass). On Bacon Channel Island (BACHI), the overstory is dominated by *Salix lasiolepis* (arroyo willow), and the understory is dominated by *Cornus sericea* (red osier dogwood) with smaller amounts of *Phragmites australis* (common reed) and *Rosa californica* (California wild rose). On Franks Wetland (FW), the vegetation is dominated by *C. sericea* and *S. lasiolepis*, with the coring site having a large population of *Athyrium filix-femina* (western lady fern). The tip of Mandeville Tip (TT) is dominated by *C. sericea* and *S. lasiolepis*. Several species such as *Schoenoplectus acutus* (hard-stem bulrush), *P. australis*, and *Typha* spp. are found at all sites. All botanical nomenclature follows Hickman (1993).

Methods

Field Work

In the summer of 2005, peat cores from the marsh islands and farmed islands were retrieved using a modified 5-cm-diameter Livingstone corer (Wright 1991). Cores were collected in multiple drives all the way to refusal in the underlying mineral sediment to ensure that the entire peat column was retrieved. Total peat thicknesses are shown in Table 2. At BRI, the first core, BRIC4, did not have good recovery near the surface due to a dense root mat. In addition, BRIC4, which was 775 cm, did not reach the

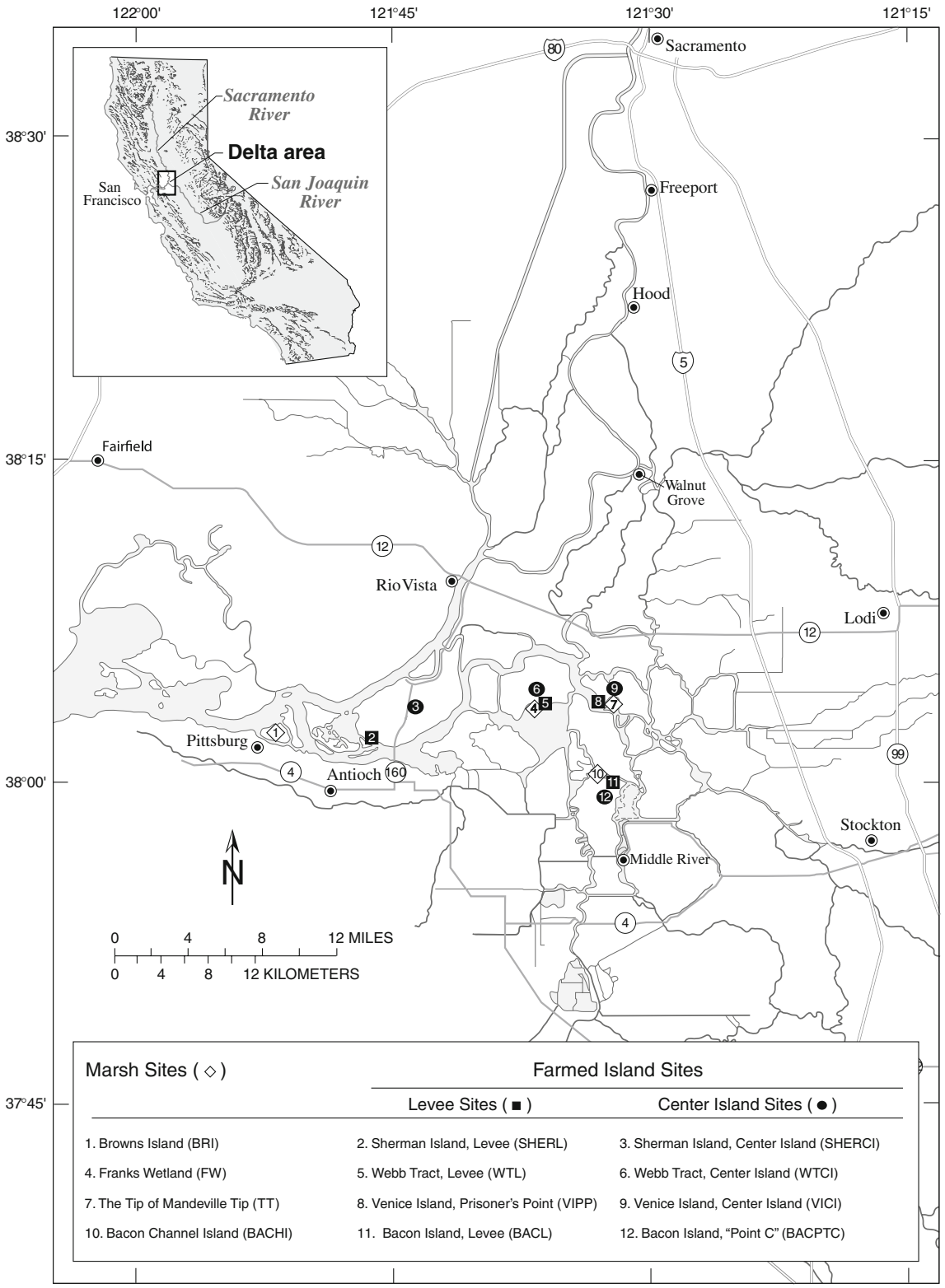

Fig. 1 Location and site map of the Sacramento–San Joaquin Delta, CA, USA. The legend contains all coring locations and names of each of the farm and marsh sites in the study

Table 1 Basic descriptions of coring sites in the delta

Coring site name	Island size (ha)	Elevation relative to MSL (m)	Salinity regime in channel	Hydrogeomorphic setting	Relative energy regime	Period of drainage and levee building
Browns Island (BRI)	268	0.51	Mixohaline	Confluence of SR and SJR	High	NA
Sherman Island, levee (SHERL)	4,205	−4.44	Mixohaline	Confluence of SR and SJR	High	1870–1880
Sherman Island, Center Island (SHERCI)	4,205	−4.52	Mixohaline	Confluence of SR and SJR	High	1870–1880
Franks Wetland (FW)	28	0.27	Fresh	Distributary of SJR, sheltered by natural marsh breakwaters, adjacent to permanently flooded farmed island	Very low	NA
Webb Tract, Levee (WTL)	2,205	−5.18	Fresh	Main channel SJR and within historic floodplain of SR	Medium	1910–1920
Webb Tract, Center Island (WTCI)	2,205	−7.25	Fresh	Main channel SJR within historic floodplain of SR	Medium to low	1910–1920
The Tip of Mandeville Tip (TT)	12	0.20	Fresh	Glacial outwash region in main channel of SJR	Medium	NA
Venice Island Prisoners' Point, levee (VIPP)	1,263	−4.52	Fresh	Glacial outwash region in main channel of SJR	Medium	1900–1910
Venice Island, Center Island (VICI)	1,263	−6.95	Fresh	Glacial outwash region in main channel of SJR	Medium to low	1900–1910
Bacon Channel Island (BACHI)	10	0.21	Fresh	Glacial outwash region along distributary of SJR	Low	NA
Bacon Island, Levee (BACL)	2,257	−5.86	Fresh	Glacial outwash region along distributary of SJR	Low	1910–1920
Bacon Island, "Point C" (BACPTC)	2,257	−6.28	Fresh	Glacial outwash region along distributary of SJR	Low	1910–1920

Salinity data represent typical nondrought conditions in adjacent sloughs and are based on Atwater (1980). Mixohaline (brackish) refers to a range of approximately 0–10 ppt, with higher salinities found during the dry season. Terminology follows Mitsch and Gosselink (2000). Descriptions of hydrogeomorphic settings follow those described in Atwater (1980)

SR Sacramento River, *SJR* San Joaquin River, *NA* not applicable

Table 2 Peat thicknesses and ages and depths of basal peat from each of the coring sites

Coring site	Peat thickness (cm)	Elevation relative to MSL (cm)	CAMS lab code	Radiocarbon age (^{14}C year BP)	Calibrated age (cal year BP)	Macrofossil type[a]
BRI[b]	912	−861	133146	5,600±70	6,233 (6,031–6,293)	Achenes
SHERL[c]	317	−761	126714	5,670±35	6,450 (6,325–6,550)	Achenes
SHERL[c]	317	−761	126724	5,740±70	6,540 (6,360–6,720)	Charcoal
SHERCI[c]	243	−695	126713	5,425±40	6,235 (6,035–6,300)	Achenes
FW[d]	608	−580	126712	4,340±40	5,440 (5,327–5,575)	Achenes
WTL[c]	350	−868	126719	5,830±40	6,645 (6,505–6,740)	Achenes
WTL[c]	350	−868	126728	5,905±30	6,720 (6,665–6,790)	Charcoal
WTCI[c]	184	−909	126718	5,800±35	6,600 (6,495–6,710)	Achenes
TT	424	−404	126715	2,315±35	2,340 (2,160–2,435)	Achenes
VIPP[c]	378	−830	126717	5,790±35	6,590 (6,495–6,670)	Achenes
VICI[c]	198	−893	126716	5,870±35	6,695 (6,570–6,785)	Achenes
BACHI	726	−705	126819	5,085±40	5,820 (5,740–5,915)	Achenes
BACL[c]	257	−843	126709	5,680±35	6,460 (6,355–6,560)	Achenes
BACPTC[c]	160	−788	126710	5,475±35	6,280 (6,200–6,390)	Achenes
BACPTC[c]	160	−788	126721	5,445±35	6,245 (6,190–6,300)	Charcoal

Duplicate dates are available for some sites where radiocarbon analyses were done on multiple macrofossil types for the same depth interval. Calibrated ages are the median of the 2σ probability distribution (2σ ranges in parentheses) calculated by CALIB (Stuiver and Reimer 1993, v5.0.1)

CAMS Center for Accelerator Mass Spectrometry at Lawrence Livermore National Laboratory

[a] All of the achenes analyzed were *Schoenoplectus* spp.

[b] The macrofossil is from 912 cm, while the peat column extends to 922 cm

[c] These coring sites were on drained farmed islands subject to compaction and major land surface subsidence

[d] Signifies the deepest date in the peat column before a series of age reversals extending to 718 cm in depth

underlying mineral substrate, even though much clay was already present below 700 cm. Therefore, an additional core of peat thickness 922 cm was collected in March of 2007 within 2 m of the original coring site. A soil monolith of 49 cm was excavated from the surface in order to improve surface recovery.

Core drives were extruded onto cellophane-lined polyvinyl chloride (PVC) tubes cut longitudinally in half, photographed, and visually described in the field regarding color and texture. The cores were quickly wrapped in cellophane, covered with the other longitudinal half of the PVC tube, and taped shut. All cores were immediately placed in a large cooler and subsequently transported to the laboratory where they were stored in a refrigerator at approximately 3°C.

Real-time kinematic (RTK) geographic positioning was used to establish the elevations and coordinates of the coring locations. Full details of the RTK survey can be found in Drexler et al. (2009). Ellipsoid heights from the RTK survey were converted to orthometric elevations (NAVD88) using a GEOID03 model. Tidal benchmark LSS 13 (NOAA tidal station 9415064 on the San Joaquin River near Antioch, CA, USA) with a static surveyed ellipsoid height of −28.75 m was used to adjust the elevations of the coring sites to local mean sea level (MSL). Based on the height difference of 14 overlapping survey points from different base stations, the error of the core site elevations is estimated to be ±0.075 m.

Laboratory Work

In the laboratory, cores were individually unwrapped, split lengthwise, and immediately photographed. Core stratigraphy was documented, and one longitudinal half of the core was wrapped in cellophane and archived for future use. Bulk density was obtained by sectioning cores into 2-cm-thick blocks, measuring each dimension, obtaining wet weight of the sample, drying overnight at 105°C, and then weighing again to obtain dry weight (Givelet et al. 2004). Core data were examined for compression and/or expansion, but no mathematical corrections were needed. The only correction made was to remove a small amount of peat from the top and bottom of some drives (generally <4 cm) when it was visually apparent that the drives contained noncontiguous peat from elsewhere in the core. The presence of noncontiguous peat was confirmed in the

laboratory by anomalous bulk density values that differed from the rest of the drive. The peat monolith from BRI expanded slightly upon removal from the marsh surface. The amount of expansion was determined, and the core data were corrected accordingly. Basal contacts of the peat columns with the underlying epiclastic sediment were generally sharp and could usually be determined by a spike in bulk density for sections immediately beneath the peat. At one site (BRI), however, the transition from peat to epiclastic sediment was gradual. Therefore, we also used the definition of an organic soil to differentiate peat from underlying mineral sediments. Saturated organic soils by definition must have an organic carbon (OC) content (by weight) of (1) >18% if the mineral fraction has 60% or more clay, (2) >12% if the mineral fraction contains no clay, or (3) >12% + (clay percentage multiplied by 0.1%) if the mineral fraction contains less than 60% clay (US Department of Agriculture Soil Conservation Service 2006).

To determine percent OM, standard loss on ignition (LOI) procedures were followed in which the dried bulk density samples were milled and heated to 550°C for 4 h (Heiri et al. 2001). LOI was analyzed at 4-cm intervals both at the top meter of the core and at the bottom meter before contact with the epiclastic sediment underlying the peat. At all other places in the cores, LOI was conducted at 10-cm intervals. On average, a duplicate LOI sample was run for every 9.5 samples. Mean error for duplicates (error= absolute value (duplicate A−duplicate B)/(larger of A or B)× 100) was 0.74% (range=0.00–4.8%). Nine hundred samples were processed for LOI.

Total carbon was determined for 100 samples by the Department of Agriculture and Natural Resources (ANR) laboratory at the University of California, Davis (AOAC International 1997, Method 972.43). The samples were randomly selected from within each 1-m core segment of each core from every site. To avoid possible contamination, samples were not selected from the upper and lower 10 cm of each drive. For quality assurance, 13 blind samples were also submitted to complement the 14 duplicates run by the ANR lab as part of their quality control procedure. Duplicates averaged within 1.2% of their original total carbon sample. Several samples with the highest bulk density from each site were selected (for a total of 29 samples) and analyzed for carbonate following the method of the US Salinity Laboratory Staff (1954). A mineral sediment sample within 22 cm of the contact with the overlying peat was included in this analysis for 11 of the sites to determine whether the mineral sediment could be a significant source of carbonate within the peat. The mineral sediment contained an average of less than 0.2% carbonate and the peat samples had an average of less than 0.4% carbonate, indicating that total percent carbon accurately approximates the percent OC of the peat. LOI values were converted to OC values using a regression in which OC= 0.55(OM)−2.69 (where OM = organic matter, r^2=0.98, p<0.0003).

Organic fragments for radiocarbon analysis were sampled directly from the split core face where visible, or a 2- to 4-cm-thick sample of peat was sieved to concentrate seeds, charcoal, or other terrestrial macrofossils. *Schoenoplectus* achenes in particular were sought out as these were well distributed in the peat cores and have been shown to be a reliable material for radiocarbon dating of peat layers (Wells 1995). The majority of the achene samples were identified as *S. acutus* var. *occidentalis*. Radiocarbon samples were analyzed by accelerator mass spectrometry (AMS) at the Center for Accelerator Mass Spectrometry (CAMS), Lawrence Livermore National Laboratory (LLNL) in Livermore, California. Ages were calibrated using CALIB (version 5.0.1 (Stuiver and Reimer 1993) with the INTCAL04 curve (Reimer et al. 2004)). All details related to the radiocarbon data used in this study are shown in "Appendix."

Test for Autocompaction

In order to test for autocompaction, we focused on the change in porosity with depth in the peat column. Previous research has indicated that peats with porosities greater than 75% are "poorly compacted" (Kaye and Barghoorn 1964). We calculated particle densities of peat (ρ_o) using the empirical equation by Okruszko (1971) who studied nearly 3,000 peat samples from a variety of peatlands with ash contents ranging from 0.7% to 99.5%:

$$\rho_o = 0.011\ (\mathrm{IM}) + 1.451\left(\mathrm{g\ cm^{-3}}\right) \quad (1)$$

where inorganic matter (IM)=percent ash content. The following equation from Hillel (1998) was used to calculate porosity Φ (%):

$$\Phi = 1 - (\mathrm{BD}/\rho_o) \quad (2)$$

where BD = bulk density (g cm^{-3}) of marsh peat at a particular depth.

Inorganic vs. Organic Contribution to Soil Volume

The relative contributions of OM vs. IM to soil volume (OM_v and IM_v, respectively) were calculated as follows:

$$\%\ \mathrm{OM_v} = (\mathrm{BD} \times \mathrm{LOI})/1.45 \quad (3)$$

$$\%\ \mathrm{IM_v} = (\mathrm{BD} \times (100 - \mathrm{LOI}))/2.61 \quad (4)$$

where LOI is loss on ignition in percent; 1.45 g cm^{-3} is the particle density of OM in peat and 2.61 g cm^{-3} is the particle density of inorganic sediment in peat. DeLaune et

al. (1983) measured the particle density of IM in peat and found it to be 2.61, which is essentially the commonly used average value of 2.6 for inorganic sediment (McKensie et al. 2002.) The particle density value of "1.45" for OM in peat was calculated using Eq. 1. This value was also checked against particle density values in the literature and found to be very similar to sedge peat measured by Redding and Devito (2006).

Statistical Analysis

Cubic smooth spline regression models (hereafter, spline fit models) for BRI, FW, and BACHI were constructed following the statistical approach of Heegaard et al. (2005), who used a mixed-effect regression model in order to incorporate (1) an error estimate for each individual object (within-object variability of dated macrofossils) and (2) an error estimate for how representative each dated object is in relation to the sampled layer (between-object variability). This approach also includes a loess smoothing procedure which combines linear least squares regression with nonlinear polynomial regression by fitting simple models to localized subsets of the data. For each marsh data set, diagnostic plots (residuals vs. fitted, square root of absolute residuals vs. fitted, observed versus fitted, and a qq-normplot) were examined to assess normal distribution of data and residuals. These plots together with variance plots were also examined in order to determine whether a constant variance or a μ variance was a better choice for the data. The median of the calibrated age distributions for the various macrofossils was used in the age–depth models. When multiple dates were available for a particular depth, *Schoenoplectus* achenes were preferentially chosen due to their proven dependability in dating peat layers (Wells 1995). Radiocarbon dates for which the "between-object" variability was large in comparison to the "within-object" variability were identified as possible outliers (Heegaard et al. 2005). Such outliers, which indicate an inversion in the stratigraphy or a discontinuity with depth, were closely examined and only removed from the data set when they were notably different from any other nearby data points. Several iterations of each age–depth model were carried out in order to determine what level of smoothing was needed to best represent the overall shape of the curve. The resulting age–depth models were constructed with 95% confidence envelopes. It is important to note that, with this approach, the greater the radiocarbon data set (n), the greater is the confidence in the resulting spline fit model (Heegaard et al. 2005). The age–depth models were used to estimate accretion rates for each centimeter of the peat column. A 95% confidence envelope for the accretion rate estimates was determined using the Delta method, which is based on a Taylor series approximation (Miller 1998).

Results

The radiocarbon data, when plotted by depth from the peat surface, form two main groups, which are largely linearly distributed (Fig. 2a). The first group consists of the marsh sites and is found on the right side of Fig. 2a. The second group consists of the farmed sites and is situated on the upper left of Fig. 2a. The top of the peat column from the farmed islands has been lost primarily due to microbial oxidation of peat subsequent to drainage for agriculture, making the peat column much thinner and older than at the marsh sites. Radiocarbon data from Shlemon and Begg (1975), shown in Fig. 2a, straddle the data from this study. More of their data points occur to the right of the main line, indicating slightly younger ages of the bulk peat samples used in their study. Below 1,000 cm, the dates reported by Shlemon and Begg (1975), which are for Sherman Island at depths of 1,220 and 1,520 cm below land surface, seem improbably old for peat per se (see definition for organic soil in "Laboratory Work") but highly possible for organic silts and clays found below the peat column. The oldest peats in this study are from Webb Tract Levee, Webb Tract Center Island, Venice Island Prisoner's Point, and Venice Island Center Island and date to approximately 6,600–6,700 years BP (median values; Table 2). In Fig. 2b, all the radiocarbon data are plotted relative to MSL. Figure 2b also includes radiocarbon data from Atwater et al. (1977) for plant roots, plant fragments, and other organic materials from south San Francisco Bay.

Spline fit models were constructed for the marsh sites FW, BRI, and BACHI, and a linear model was determined for TT, which had too few data points for a spline fit (Fig. 3). Spline fit models were not constructed for the subsided farmed islands because most of the peat column has been lost and the remaining peat is highly compacted, precluding its use in estimating accretion rates. Diagnostic and variance plots indicated that constant variance was the best fit for each of the three cubic smooth spline regressions. For each of the resulting spline fit models, the estimated ages are shown up until 250 years BP or the most modern sample date available. More recent radiocarbon samples were not analyzed as such ages are difficult to interpret conclusively unless intensive techniques such as wiggle matching of closely spaced samples are employed (Turetsky et al. 2004). For FW, the spline fit model fluctuates slightly in slope within the top 5.8 m MSL of the peat record. Below 5.8 m in elevation, there were major age reversals in the stratigraphy from FW, and, therefore, these data were omitted from the age–depth model. The model for BRI, on the other hand, has a less linear pattern, with major increases in slope between −4.0 to −6.0 m and −8.5 to −9.0 m in depth relative to MSL. The transition from core 4 to core 5 shows two points that fall outside the

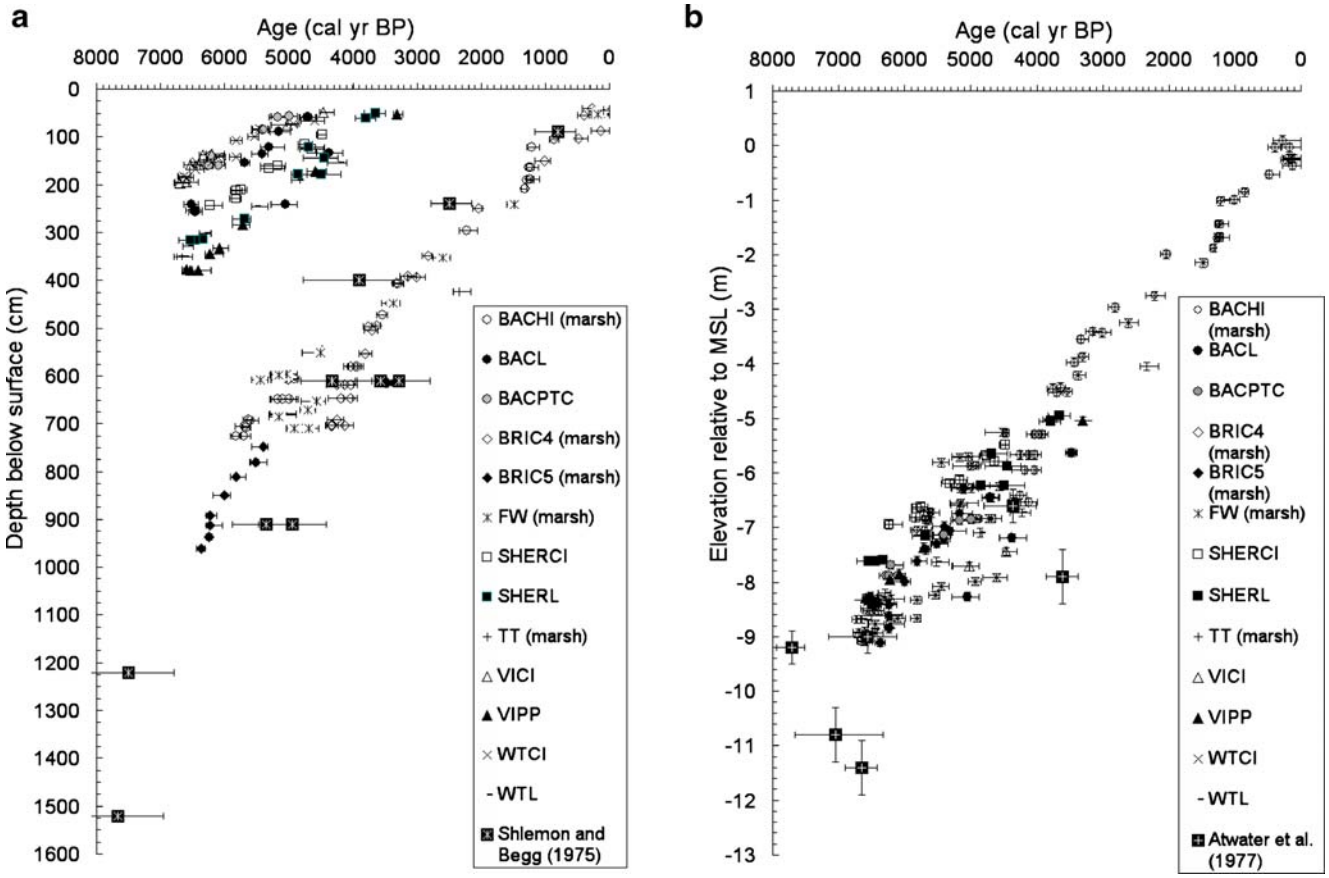

Fig. 2 Radiocarbon data in calibrated years before present (cal year BP) for all cores presented by **a** depth below surface and **b** elevation relative to local MSL. Each data point is the median probability of the 2σ range. The *x-axis error bars* encompass the minimum and maximum 2σ range. *Y-axis error bars* are not shown in part **a** because error is on the order of a few millimeters for this study. *Error bars* for depth relative to MSL in part **b** incorporate the error estimates from the RTK GPS survey and Atwater et al. (1977). Radiocarbon dates from Shlemon and Begg (1975) and Atwater et al. (1977) are shown separately in plots **a** and **b** due to their use of depth below land surface vs. elevation relative to MSL, respectively, as reference points for elevation. Details for each radiocarbon sample are provided in "Appendix"

95% confidence interval at −5.61 and −6.25 m. There is some uncertainty regarding the actual slope of the spline fit model between approximately −6.5 and −7.0 m because there were few radiocarbon samples available at this important junction between the two cores. The age–depth model for BACHI also departs from linearity. There are two depth ranges, between approximately −1.5 to −2.0 m and −4.0 to −4.5 m relative to MSL, where sharp increases in slope are found.

The core from FW was chosen to check for autocompaction via changes in porosity because it had a high OM content from top to bottom (Drexler et al. 2009). A high organic content indicates that the core is theoretically highly compressible (Kaye and Barghoorn 1964). Overall, the average porosity for FW between 0.8 and 5.8 m below MSL decreases slightly from approximately 96% to 94% (data within oval, Fig. 4). Such high porosity values decreasing only slightly with depth indicate that autocompaction is probably minimal. The zones of lower porosity near the marsh surface are due to increased inorganic sediments and the lower porosities below −5.8 m reflect the increase in epiclastic sediments near the bottom of the peat column (Drexler et al. 2009). Such an apparent lack of autocompaction in the FW core suggests that the other marsh cores, which have similar or less organic content, are also largely free from autocompaction. However, we cannot be sure that there is no autocompaction in Delta peat because we have no data on other aspects of autocompaction such as the collapse of plant fibers and decomposition effects (Kaye and Barghoorn 1964; Allen 2000). Therefore, vertical accretion rates reported here will be considered conservative estimates.

Yearly accretion estimates were calculated based on the spline fit models shown in Fig. 3 for FW, BRI, and BACHI (Fig. 5, Table 3). For TT, accretion was calculated linearly between 100 and 1,210 cal year BP (0.13 cm year^{-1}) and between 2,340 and 1,210 cal year BP (0.21 cm year^{-1}). FW has the least variable and lowest estimated mean accretion

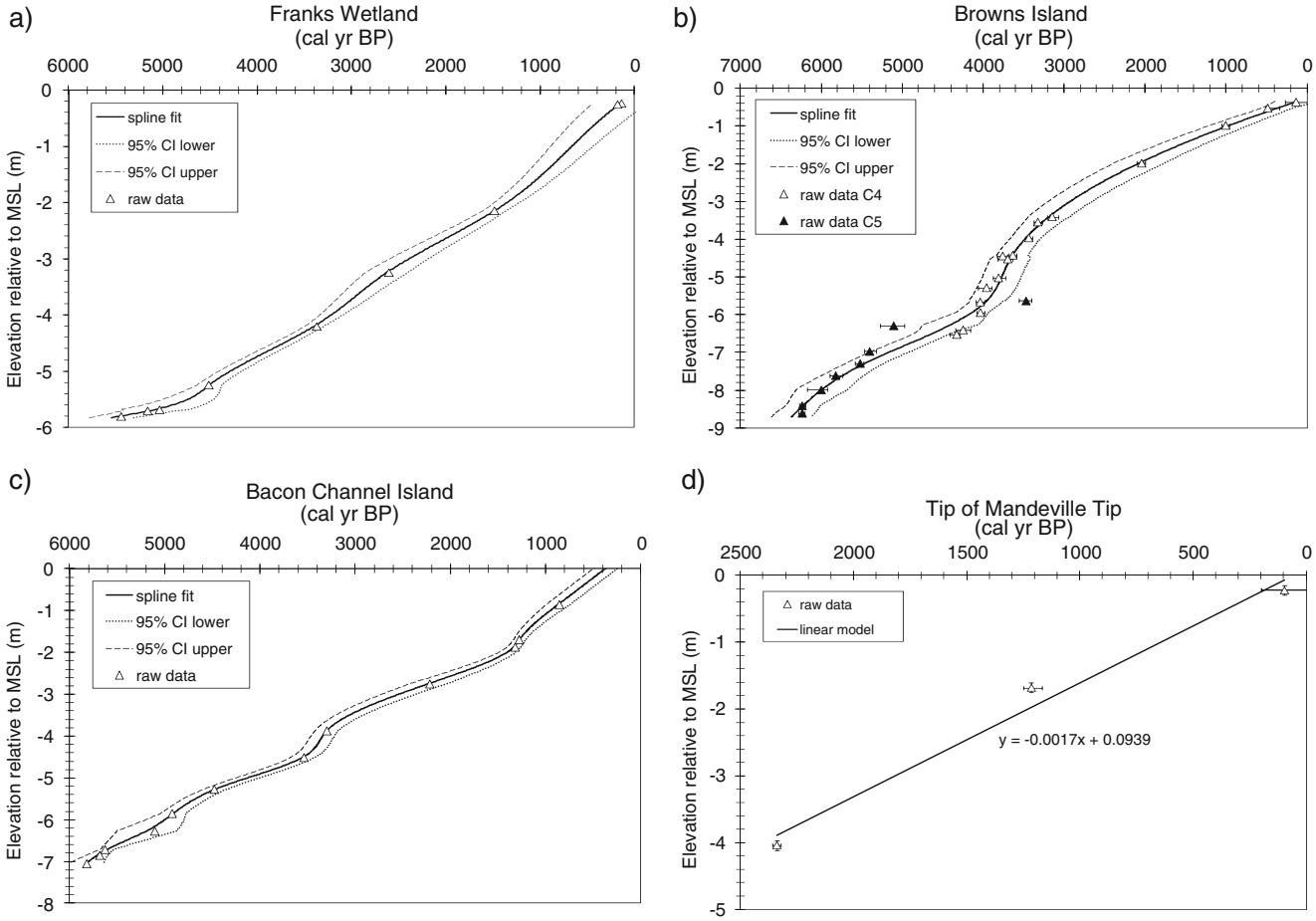

Fig. 3 Spline fit age–depth models are shown for **a** FW (n=9), **b** BRI (n=24), and **c** BACHI (n=12). For each marsh data set, diagnostic plots (residuals vs. fitted, square root of absolute residuals vs. fitted, observed versus fitted, and a qq-normplot) were examined to assess normal distribution of data and residuals. A linear model, **d**, is shown for TT. The model for FW ends at −5.8 m relative to MSL because of major age reversals below this depth. The plot for BRI contains data from both core 4 and core 5 collected at the site

rate (0.12 cm year^{-1}, SD=0.03), while BRI has the most variable and highest estimated mean accretion rate (0.18 cm year^{-1}, SD=0.11). For FW, there are gently alternating periods of higher and lower estimated accretion rates that range between 0.03 and 0.16 cm year^{-1}. BRI has two periods of high estimated accretion rates: (1) near the core bottom and (2) between −4.0 and −5.5 m relative to MSL. BACHI also has variable estimated accretion rates (0.07–0.38 cm year^{-1}, Table 3), with two major peaks at approximately −1.7 and −4.1 m MSL.

The marsh peats form two basic groups, FW and BACHI vs. BRI and TT, based on their physical characteristics. In the first group, mean percent OM is greater than 70% and mean bulk density is less than <0.15 g cm^{-3} (Table 4). With respect to the organic and inorganic contributions to soil volume (OM_v and IM_v, respectively), mean OM_v contributes about twice as much as IM_v to soil volume at FW and mean OM_v contributes almost four times more than IM_v to soil volume at BACHI (Fig. 6). In contrast, mean percent OM at BRI and TT is approximately 40% and mean bulk density is 0.31 and 0.23 g cm^{-3}, respectively (Table 4). The mean contributions of OM_v relative to IM_v are similar for both BRI and TT (Fig. 6). Below approximately 1 m relative to MSL in both the BACHI and FW cores, IM_v is less than ~3% until the bottom of the peat column (Fig. 6). In contrast, at BRI and TT, IM_v is much more variable with depth in the peat column (Fig. 6). IM_v reaches over 15% at midcore at BRI and below the contact with epiclastic sediment in all cores (not shown). Both IM_v and OM_v increase toward the marsh surface at all marsh sites (Fig. 6).

Discussion

Peat Formation and Subsidence

The oldest basal peats from this study date to ~6,600–6,700 cal year BP (median values; Table 2). These results

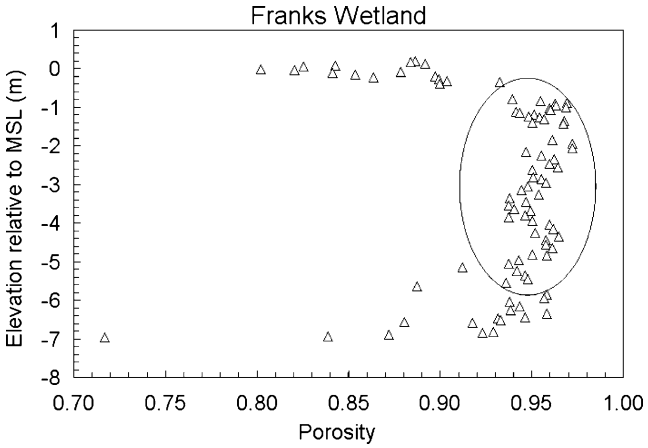

Fig. 4 Calculated porosity vs. elevation relative to MSL (m) at FW. The porosity values within the *oval* were used to assess the degree of autocompaction in the peat

suggest that peat started forming in the central and western Delta when sea level rose and finally inundated the large flat pre-Holocene valley at the landward end of the San Francisco Bay Estuary (Fig. 2, Table 2). In their 1975 paper, Shlemon and Begg came to another conclusion; namely, that peat initially formed on the western edge of the current Delta and spread easterly across the rest of the region. They came to this conclusion, however, based on the evidence of ten radiocarbon dates spread across the Delta and one basal peat date from Sherman Island only. Their basal peat date from Sherman Island is older (median age of 7,668 cal year BP) than what was found in this study. This older date is certainly possible because older and deeper pockets of pure freshwater peat may have formed before encroachment by sea level rise and may still underlie the continuous layer of peat in the current Delta. In addition, it is also possible that this date refers not to peat per se but instead to organic material incorporated in organic muds or lacustrine sediments found beneath the peat column (personal communication, Roy Shlemon). This basal date for Sherman Island is coexistent with some marsh deposits from San Francisco Bay (Atwater et al. 1977, Fig. 2b). Marshes in San Francisco Bay, however, most likely formed before Delta marshes due to the lower elevation of the bay relative to the Delta and the proximity of the bay to the Pacific Ocean. Therefore, considering the data available, it appears that peat deposits in the Delta started forming ~6,700 years ago, which is consistent with the stabilization of sea level about 6,000–8,000 years ago when many other deltas and associated wetlands started forming around the world (Stanley and Warne 1994).

Peat profiles of the radiocarbon data provide an unusual perspective regarding the legacy of draining marshes for agriculture (Fig. 2a). In Fig. 2, peat ages from the farmed islands fall into an entirely different group from the marsh islands because the top 3,000+ years worth of accretion (approximately two thirds of the peat column) have been lost primarily due to peat oxidation subsequent to drainage for agriculture (Fig. 2; Drexler et al. 2009). Much of the remaining peat on the farmed islands has also been shown to be compacted, mainly as a result of the initial settling of the soil after drainage (Drexler et al. 2009). For these reasons, radiocarbon dates from the farmed islands could

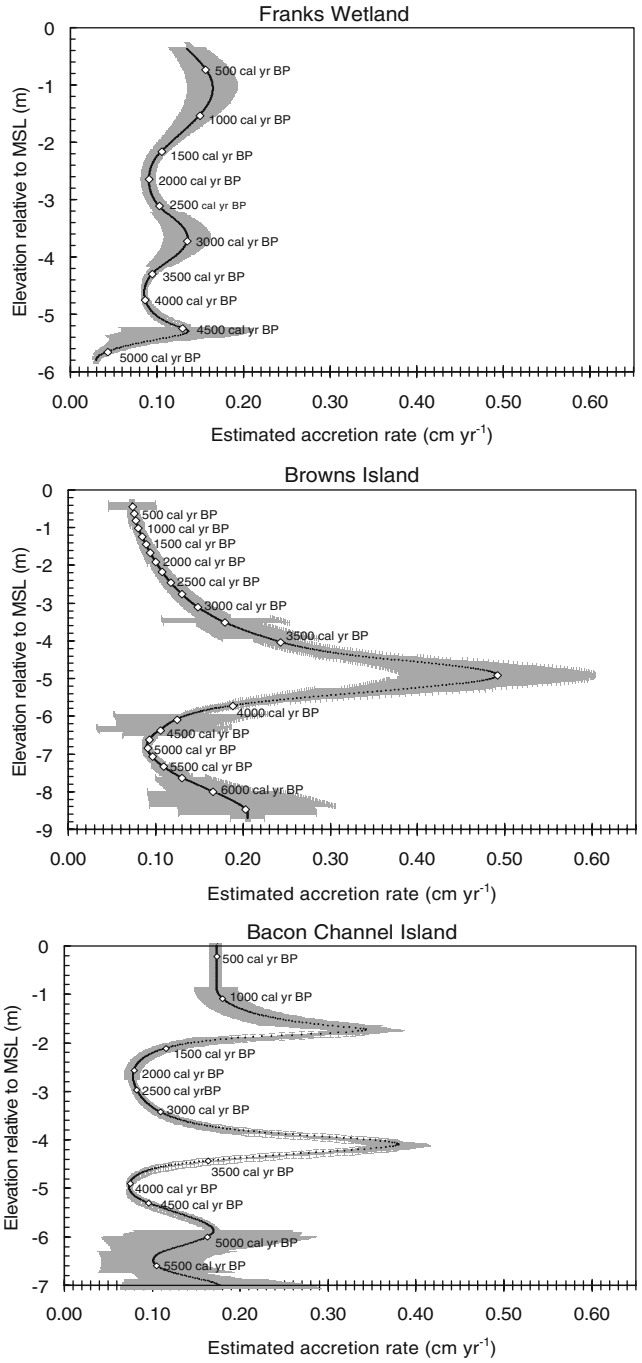

Fig. 5 Estimated yearly vertical accretion rates calculated from the spline fit models for FW, BRI, and BACHI. The 95% confidence envelopes were determined using the Delta method (see text)

Table 3 Estimated vertical accretion rates for the marsh sites compared with Holocene average rates and twentieth century global rates of sea level rise in centimeter per year

Site and model type	Estimated range, mean, and SD of accretion for the entire peat column based on age–depth models	Estimated sea level rise in the San Francisco Bay Estuary from 6,000 years ago to present (Atwater et al. 1977)	Twentieth century estimated rate of global sea level rise (Church and White 2006)
BRI (spline fit)	(0.07–0.49), 0.18, 0.11	0.1–0.2	0.17±0.03
BACHI (spline fit)	(0.07–0.38), 0.16, 0.07	0.1–0.2	0.17±0.03
FW[a] (spline fit)	(0.03–0.16), 0.12, 0.03	0.1–0.2	0.17±0.03
TT (linear model using 3 data points)	Two estimates available: 0.13[b] between 100 and 1,210 cal year BP 0.21[b] between 1,210 and 2,340 cal year BP	0.1–0.2	0.17±0.03

[a] Mean accretion rate calculated only to −5.8 m MSL due to age reversals below this depth

[b] Represents median of the 2σ range (for error bars, see Fig. 3)

not be used to construct age–depth models or estimate vertical accretion rates.

Vertical Accretion

Rates of vertical accretion per year were estimated from the spline fit models for FW, BRI, and BACHI (Fig. 5). It is important to note that the greater the number of radiocarbon dates for each site (n), the lesser is the uncertainty of the resulting spline fit models (Heegaard et al. 2005) and, hence, the better are the estimates of accretion. Therefore, BRI (n=27) has better estimates relative to FW (n=9) and BACHI (n=12). However, there is a section in the BRI spline fit model between approximately −6.5 and −7.0 m that has greater uncertainty than the rest of the model. This is due to some heterogeneity between the two cores that were used to construct the model and the fact that there were limited radiocarbon samples available in this depth range. Despite any limitations, however, the construction of spline fit age–depth models and the estimation of yearly accretion rates are clearly an improvement over using simple linear models to produce a few sporadic estimates of accretion. Such a method of estimating accretion rates permits a rare view into the accretion history of these marshes through the millennia.

Table 4 Mean bulk density and mean percent OM (±standard deviations) for marsh cores

Core	Mean bulk density (g cm^{-3})	Mean % OM
FW	0.14±0.08	72±19
BRI	0.31±0.15	40±18
BACHI	0.12±0.05	76±16
TT	0.23±0.11	41±13

Estimated rates of peat accretion in the marsh sites ranged between 0.03 and 0.49 cm year^{-1} (Table 3). Estimated mean accretion rates at BRI, BACHI, and FW were 0.18 (SD=0.11), 0.16 (SD=0.07), and 0.12 cm year^{-1} (SD=0.03), respectively. The accretion history for TT could not be estimated because there were not enough radiocarbon data to construct a spline fit model for this site. Because some peat undoubtedly has been lost through decomposition, vegetation compaction, and loss of porosity through time (however minor, see Fig. 4), these estimates for vertical accretion are likely conservative estimates. Compared to recent rates of land surface subsidence on farmed islands in the Delta (0.5–3.0 cm year^{-1}; Rojstaczer and Deverel 1993, 1995; Deverel and Leighton 2009), estimated rates of vertical accretion are quite low. However, in comparison to other peatland types, estimated vertical accretion rates for the Delta are greater than some millennial rates in inland boreal regions (e.g., 0.05 cm year^{-1} over 6,000 year from Zoltai and Johnson 1984; 0.04–0.06 cm year^{-1} over 1,200 years from Robinson and Moore 1999) and within millennial rates in salt marshes in the northeastern USA (e.g., 0.11–0.25 cm year^{-1} over the past 4,000–5,000 years; Bloom 1964; Redfield 1967; Bartberger 1976; Keene 1971). In comparison to other tidal freshwater marshes, mean accretion rates in this study are very similar to those measured in a Pamunkey River marsh in Virginia, USA (0.15–0.17 cm year^{-1} over 3,500 years; Neubauer 2008), greater than "pre-Colonial" sedimentation in a Delaware River marsh in NJ, USA (0.04 cm year^{-1}; between approximately 2,000 and 300 years BP; Orson et al. 1990), and greater than rates in a marsh in the Patuxent River estuary in MD, USA (0.04–0.08 cm year^{-1}, between approximately 1,000 and 1,400 years BP; Khan and Brush 1994). The range of accretion rates from this study is similar to the range found by other researchers studying BRI in the

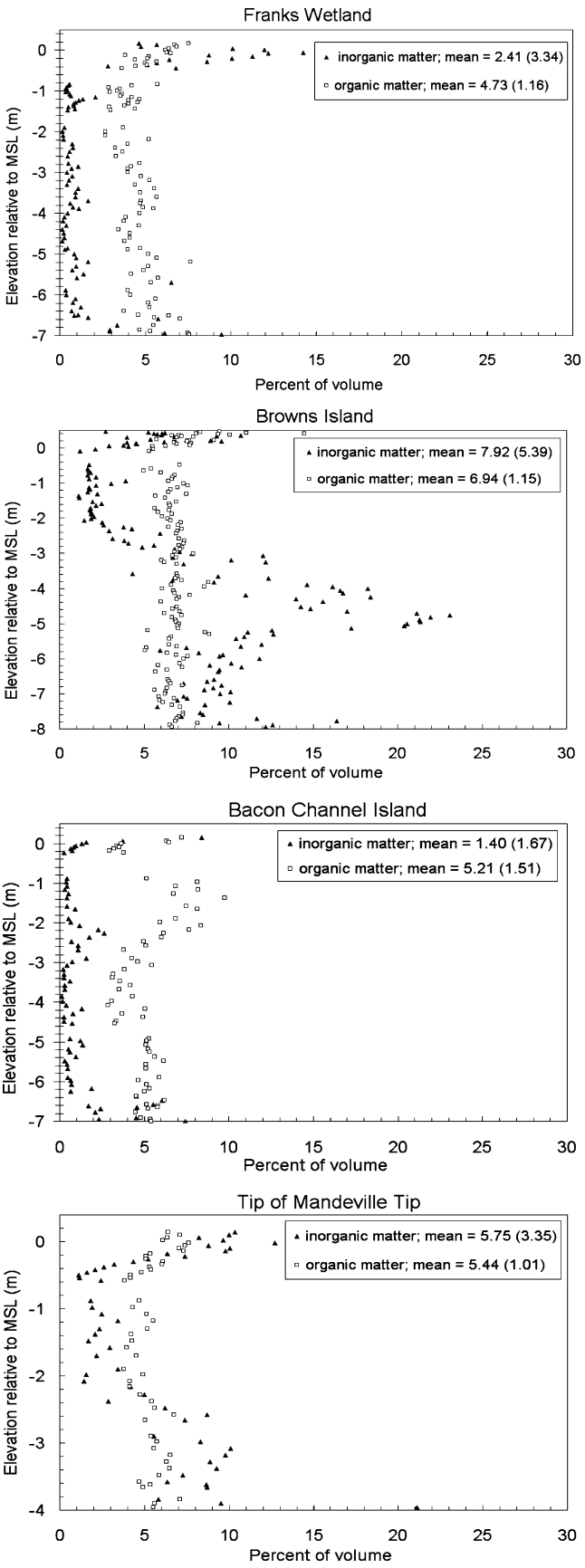

Fig. 6 Relative contribution of inorganic vs. organic matter to peat soil volume for each marsh site. The remaining void space is filled with water and/or air. Mean values for both OM_v and IM_v with standard deviations (SD) are shown in the legend for each site

Delta. Byrne et al. (2001) determined accretion rates for BRI between approximately 800 and 2,300 cal year BP and found rates between 0.05 and 0.17 cm year^{-1}. Goman and Wells (2000) determined rates for the entire peat column at BRI, and the range of their rates (0.05–0.41 cm year^{-1} over ~6,000 years) is comparable to this study. Linear age–depth models were used in both of these studies. The accretion estimates of Goman and Wells (2000) varied considerably between measurements, with the peak in accretion at BRI occurring at approximately 3,950 cal year BP instead of 3,750 cal year BP as in this study. This shift in ages may simply be due to the fact that Goman and Wells (2000) did not estimate peat age at exactly the peak of accretion or it may be due to the fact that they corrected for compaction in their cores with a core-wide linear extrapolation.

There are important differences between the marsh sites regarding vertical accretion estimates and peat characteristics. Overall, the mean estimated rate of accretion and the range of yearly accretion estimates for FW are lower than the other sites. In addition to having higher mean rates of vertical accretion, BACHI and BRI have increasingly variable patterns through time (Table 3, Fig. 5). With respect to peat characteristics, FW and BACHI both have mean OM content over 70% and bulk density below 0.15 g cm^{-3} (Table 4). In addition, for both cores, IM_v is very low through most of the peat profile (Fig. 6). These characteristics suggest that FW is a highly organic marsh site largely removed from watershed processes (i.e., sediment deposition and/or scour) and, therefore, is predominantly autochthonous with respect to peat formation. A comparison of accretion rates vs. IM_v and OM_v contributions with depth at FW shows that there are corresponding increases in both IM_v and OM_v at the major accretion peaks in the core (i.e., at depths of approximately −1.1, −3.7, and −5.3 m MSL). However, such changes are quite subtle. BACHI, with its variable accretion rate, appears to have characteristics of both an autochthonous and allochthonous site; however, due to its low IM_v, it tends more toward being autochthonous. A large increase in OM_v between approximately −1.0 and −2.25 m MSL suggests that autochthonous production at BACHI is of particular importance in this interval (Fig. 6). BRI and TT, on the other hand, have much lower mean OM content than the other marsh sites (~40%; Table 4), greater mean bulk density (0.31 and 0.23 g cm^{-3}, respectively; Table 4), and considerable variability of IM_v throughout the peat profile (Fig. 6). This suggests that BRI and TT are more responsive to watershed processes than FW and BACHI. BRI and TT

appear to alternate between periods of being allochthonous and periods of being autochthonous. In the case of BRI for which there is a spline fit model, this shift between allochthonous and autochthonous behavior corresponds directly to periods of higher and lower peat accretion (Figs. 5 and 6). Overall, IM_v is much more variable than OM_v in all of the marsh cores suggesting that much of the variability in peat accretion through time is related to changing allochthonous sediment inputs.

The variability in allochthonous sediment inputs most likely stems from climatic changes through time. The Delta region has considerable variability in precipitation rates and, thus, river flows, both seasonally and annually (Conomos 1979; Cayan and Peterson 1993). This translates into variability in the amount of suspended sediment transported to the rivers and available for peat formation. Peat accretion rates at BRI and BACHI appear to reflect dramatic increases and decreases in sediment supply over time. One period of especially high accretion rates, between approximately 4,400 and 3,100 cal year BP (Fig. 5), has been shown to be a very wet period in California history. During this time, the elevation of the tree line in the White Mountains of eastern California was over 80 m higher than the modern tree line (LaMarche 1973). Research from Mono Lake shows the beginning of an unusually high stand of the lake starting at approximately 3,800 cal year BP (Stine 1990). Even the Mojave Desert of California was especially wet during this time. Enzel et al. (1989) document the presence of an ephemeral lake that formed in the Mojave approximately 3,600 years BP.

Where a marsh falls on the autochthonous–allochthonous continuum depends largely on its hydrogeomorphic setting. Within the realm of salt marshes, autochthonous marshes are usually found in microtidal settings, while allochthonous marshes are found in settings with greater tidal range (French 2006; Allen 2000). This characterization needs to be revised for tidal freshwater marshes in the Delta because, although tidal range in the Delta can be classified as microtidal (<2 m), a slight decrease in tidal range across the Delta does not appear to have any influence over peat accretion processes. What does appear to influence peat accretion and contributions of IM_v and OM_v in the Delta is the proximity of marshes to flows in the main channels (this study and Reed 2002b), a factor shown to be directly related to accretion rates in salt and freshwater tidal marshes (e.g., Hatton et al. 1983; Merrill and Cornwell 2000). In the Delta, however, marshes situated in highly exposed, high-energy settings (i.e., BRI and TT, Table 1) have the highest accretion rates and IM_v as well as the highest variability in these values through time. These sites are most apt to be affected by major changes in river discharge and hence sediment deposition.

At all the marsh sites, there is an increase in both OM_v and IM_v to soil volume near the peat surface (Fig. 6). This may be due to the lack of consolidation of OM at the surface in comparison to deeper in the peat column. With respect to the inorganic contribution to soil volume, the increase right near the surface likely reflects the huge plug of suspended sediment carried into the Delta during hydraulic gold-mining activities in the late 1800s and early 1900s (Gilbert 1917; Orr et al. 2003).

Marsh Sustainability

Marsh sustainability is determined by the ultimate balance between marsh vertical accretion and relative sea level rise over decades and centuries and includes eustatic sea level rise and any subsidence or uplift of the land surface. An indication of the capability of a marsh to maintain its position within the tidal frame can be found by comparing mean accretion rates for marshes in this study with current and predicted rates of sea level rise. The estimated mean accretion rate of each marsh is well within the 0.1–0.2 cm $year^{-1}$ estimated rate of relative sea level rise during the past 6,000 years in the San Francisco Bay Estuary (Atwater et al. 1977) and very close to the estimated twentieth century rate of sea level rise of 0.17 cm $year^{-1}$ (SD=0.03; Church and White 2006; Fig. 4, Table 3). FW is the only site for which the mean accretion rate and the upper bound of its estimated accretion range are below the 0.17 cm $year^{-1}$ value. However, considering the uncertainties involved in both the accretion estimates for FW and the Church and White (2006) sea level rise estimate, FW is still within the error margin for keeping pace with sea level rise. The current global rate of sea level rise can be regionally adjusted by the estimated neotectonic displacement along the Midland Fault which amounts to approximately 0.4 mm $year^{-1}$ (midpoint value of 0.2 to 0.6 mm $year^{-1}$ range) of uplift on the west side of the Midland Fault (for BRI) and the same level of subsidence on the eastern side of the fault at BACHI and FW (Weber-Band 1998). Upon incorporating such displacement, the relative sea level rise becomes greater than mean vertical accretion at both FW and BACHI but not for BRI, which benefits from uplift. Under this scenario, only BRI could keep pace with current sea level rise. It is unclear, however, whether incorporating this estimate for neotectonic displacement is useful in determining how these marshes will fare with respect to sea level rise. Neotectonic activity may average approximately 0.4 mm $year^{-1}$ over a long time span in the Delta, but actual displacement can be of little or no consequence for many years and then of considerable consequence during a year with a major event (Sawai et al. 2002; Shennan et al. 1998; Witter et al. 2003). Regarding the future, all of the

estimated mean accretion rates are considerably less than the 0.38 cm year^{-1} estimate for sea level rise forecast for 2090–2099 (Intergovernmental Panel on Climate Change central estimate (scenario A1B) among six scenarios, which range from 0.15 to 0.97 cm year^{-1}; Meehl et al. 2007). This predicted central estimate, however, is still within the total range of estimated accretion rates for both BACHI and BRI (Table 3).

It is important to note that even if Delta marshes are intrinsically capable of keeping pace with sea level rise, the current availability of sediment may not be enough to keep marshes from being inundated. In the Delta as well as elsewhere, major dam construction has resulted in dramatic decreases in channel sediment loads (Yang et al. 2003; Schoellhamer et al. 2007). In the Sacramento River alone, suspended sediment concentrations have decreased approximately 50% since major dam building occurred in the 1960s (Wright and Schoellhamer 2004). Currently, it is unknown what effect this reduction in sediment availability has had on peat accretion rates in the Delta. The results from this study indicate, however, that Delta marshes depend on inputs of inorganic sediment, especially those situated in the main channels. Quantification of the recent relationships among reduced sediment loads, inorganic sedimentation rates, and peat accretion rates is, therefore, needed to better constrain predictions for marsh sustainability in the future.

Acknowledgments This study was funded by the CALFED Science Program of the State of California Resources Agency, Agreement #F-O3-RE-029. This work was performed, in part, under the auspices of the US Department of Energy by Lawrence Livermore National Laboratory under Contract DE-AC52-07NA27344. We thank Jim Orlando, Jacob Fleck, Matt Kerlin, Curt Battenfeld, Stephanie Wong, Patricia Orlando, and Nicole Lunning for their help in the field and/or lab. Greg Pasternack of the University of California, Davis generously provided laboratory facilities for much of the analyses. Michelle Sneed, Gerald Bawden, and Marti Ikehara provided critical guidance with the elevation survey. We are grateful to S. Galen Smith, Professor Emeritus, University of Wisconsin-Whitewater, for offering his help and expertise in achene identification. We also thank Anna Frampton for Polish translation and Neil Willits (Department of Statistics, UC Davis) for statistical guidance. Finally, we are thankful for the excellent reviews by Don Cahoon, Brian Atwater, and two anonymous reviewers.

Conflict of interest issues The US Geological Survey (USGS) has no financial relationship with the California Resources Agency, CALFED Science Program, which funded this research, besides the contract that was awarded to Drexler to do the work. The USGS is a public agency, and it has full control of all primary data. The authors will allow the journal to review any data from this paper if the need arises. There are no conflicts of interest to the knowledge of the authors with respect to any part of this research effort. All of the authors of this paper have contributed to, read through, and approved this paper for publication.

Appendix

Data for ^{14}C samples from all coring sites in this study

CAMS lab code	Site, core, and sample ID	Sample thickness (cm)	Sample bottom elevation (MSL in meter)	^{14}C age (^{14}C year BP)	2σ ^{14}C error (^{14}C year BP)	Median probability of 2σ range (cal year BP)	Sample material
130030	BACHIC1D2-4B	2	−0.85	960	70	857	Charcoal
128459	BACHIC1D2-12A	2	−1.01	1,265	70	1,214	Wood
128460	BACHIC1D2-33A	2	−1.43	1,315	80	1,249	Achenes
130031	BACHIC1D2-45A	2	−1.67	1,290	60	1,235	Achenes
128461	BACHIC1D2-46A	2	−1.69	1,340	60	1,279	Achenes
128462	BACHIC1D3-5B	2	−1.87	1,415	70	1,322	Wood
136897	BACHIC1D3-49A	2	−2.75	2,200	120	2,217	Plant fragment
136898	BACHIC1D5-5A	2	−3.87	3,075	70	3,298	Plant fragment
136899	BACHIC1D5-37A	2	−4.51	3,315	70	3,538	Plant fragment
128463	BACHIC1D6-25B	2	−5.27	4,005	60	4,479	Wood
128464	BACHIC1D7-4B	2	−5.85	4,350	80	4,921	Charcoal
128465	BACHIC1D7-5A	2	−5.87	4,420	70	5,003	Achenes
128466	BACHIC1D7-25A	2	−6.27	4,450	70	5,103	Achenes
128467	BACHIC1D7-47A	2	−6.71	4,890	70	5,625	Achenes
130293	BACHIC1D8-4B	2	−6.85	4,955	70	5,681	Charcoal
128468	BACHIC1D8-5A	2	−6.87	4,935	70	5,656	Achenes

CAMS lab code	Site, core, and sample ID	Sample thickness (cm)	Sample bottom elevation (MSL in meter)	^{14}C age (^{14}C year BP)	2σ ^{14}C error (^{14}C year BP)	Median probability of 2σ range (cal year BP)	Sample material
126819	BACHIC1D8-14A	2	−7.05	5,085	80	5,818	Achenes
128470	BACLC3D1-7A	2	−6.45	4,150	70	4,694	Achenes
128435	BACLC3D1-7B	2	−6.45	4,170	80	4,711	Charcoal
130032	BACLC3D1-20A,21A,22A	6	−6.75	4,470	70	5,160	Achenes
130033	BACLC3D1-37B,38A	4	−7.07	4,585	60	5,308	Charcoal
128471	BACLC3D1-44B	2	−7.19	3,940	140	4,377	Granular fragment
130294	BACLC3D1-45C	2	−7.21	4,700	70	5,407	Granular fragment
128472	BACLC3D2-6B	2	−7.41	4,960	60	5,685	Charcoal
128476	BACLC3D2-49A	2	−8.27	5,720	70	6,511	Achenes
128436	BACLC3D2-49B	2	−8.27	4,440	70	5,046	Granular fragment
128477	BACLC3D3-5Ax	2	−8.39	5,670	60	6,450	Achenes
126720	BACLC3D3-5B	2	−8.39	5,690	70	6,470	Plant fragment
126709	BACLC3D3-7A	2	−8.43	5,680	70	6,460	Achenes
128478	BACPTCC1D1-2A	2	−6.84	4,415	70	4,994	Charcoal
128479	BACPTCC1D1-3A	2	−6.86	4,495	70	5,166	Achenes
130034	BACPTCC1D1-17A	2	−7.14	4,700	80	5,413	Achenes
130295	BACPTCC1D1-17B	2	−7.14	4,645	80	5,404	Charcoal
128480	BACPTCC1D1-44A	2	−7.68	5,390	70	6,213	Achenes
126710	BACPTCC1D2-5A	2	−7.88	5,475	70	6,281	Achenes
126721	BACPTCC1D2-5B	2	−7.88	5,445	70	6,244	Charcoal
128481	BACPTCC1D2-5C	2	−7.88	5,325	70	6,101	Plant fragment
130039	BRIC4D2-8A	2	0.10	235	70	277	Achenes
128482	BRIC4D2-15A	2	−0.04	165	70	174	Achenes
128437	BRIC4D2-15C	2	−0.04	350	70	398	Plant fragment
130040	BRIC4D3-7A	2	−0.37	135	80	137	Achenes
128483	BRIC4D4-3A	2	−0.53	420	70	487	Achenes
130041	BRIC4D4-26A	2	−0.99	1,095	90	1,006	Achenes
136900	BRIC4D525A-C,26A	4	−1.99	2,075	60	2,045	Seed, charcoal, insect, seed
128484	BRIC4D6-47A	2	−3.41	2,970	70	3,151	Achenes
128485	BRIC4D6-48A	2	−3.43	2,875	70	3,002	Plant fragment
128486	BRIC4D7-4A	2	−3.55	3,100	70	3,328	Achenes
130043	BRIC4D7-25A	2	−3.97	3,225	70	3,440	Achenes
128487	BRIC4D7-48A	2	−4.43	3,390	60	3,637	Achenes
128488	BRIC4D7-49A	2	−4.45	3,485	70	3,762	Achenes
128489	BRIC4D8-3A	2	−4.53	3,440	70	3,700	Achenes
133384	BRIC4D8-28A	2	−5.03	3,535	70	3,814	Charcoal
128490	BRIC4D8-41B	2	−5.29	3,615	70	3,925	Plant fragment
128491	BRIC4D8-41C	2	−5.29	3,645	70	3,962	Charcoal
128438	BRIC4D8-41D	2	−5.29	3,705	70	4,042	Plant fragment
126711	BRIC4D9-9A-C,10A	4	−5.67	3,840	80	4,254	Achenes
126722	BRIC4D9-10B	2	−5.67	3,705	60	4,040	Charcoal
126723	BRIC4D9-10C	2	−5.67	3,765	70	4,130	Plant fragment
130044	BRIC4D9-24A	2	−5.95	3,700	70	4,038	Achenes
130296	BRIC4D9-24C	2	−5.95	3,800	70	4,188	Plant fragment
130045	BRIC4D9-47A	2	−6.41	3,840	70	4,252	Achenes

CAMS lab code	Site, core, and sample ID	Sample thickness (cm)	Sample bottom elevation (MSL in meter)	^{14}C age (^{14}C year BP)	2σ ^{14}C error (^{14}C year BP)	Median probability of 2σ range (cal year BP)	Sample material
130046	BRIC4D10-3A	2	−6.53	3,890	70	4,330	Achenes
130297	BRIC4D10-3C	2	−6.53	3,765	60	4,129	Charcoal
130298	BRIC4D10-3D	2	−6.53	3,910	70	4,346	Plant fragment
133137	BRIC5D8-8A	2	−5.63	3,250	70	3,469	Achenes
133138	BRIC5D8-8B	2	−5.63	3,265	70	3,492	Charcoal
133139	BRIC5D8-40A,41A	4	−6.29	4,450	70	5,103	Achenes
133140	BRIC5D9-25A	2	−6.97	4,680	70	5,400	Achenes
133385	BRIC5D9-41A	2	−7.29	4,790	70	5,518	Achenes
133386	BRIC5D9-41B	2	−7.29	4,810	70	5,520	Charcoal
133141	BRIC5D10-7A	2	−7.61	5,050	70	5,819	Achenes
133142	BRIC5D10-26A	2	−7.99	5,240	90	5,998	Achenes
133143	BRIC5D10-47A	2	−8.41	5,405	60	6,234	Achenes
133144	BRIC5D11-7A	2	−8.61	5,410	70	6,233	Achenes
128492	FWC2D1-25A	2	−0.23	140	60	142	Achenes
128493	FWC2D1-26A	2	−0.25	215	70	184	Plant fragment
130299	FWC2D3-21B	2	−2.15	1,610	80	1,488	Plant fragment
130049	FWC2D4-26B	2	−3.25	2,530	80	2,606	Charcoal
130050	FWC2D5-23A,24A	4	−4.21	3,140	70	3,370	Charcoal
130051	FWC2D6-26A	2	−5.25	4,040	80	4,513	Achenes
130052	FWC2D6-48A	2	−5.69	4,435	70	5,034	Achenes
128494	FWC2D6-49A	2	−5.71	4,470	70	5,160	Achenes
128495	FWC2D7-4A	2	−5.81	4,710	70	5,440	Achenes
130053	FWC2D7-26A	2	−6.25	4,070	70	4,561	Achenes
128496	FWC2D7-36A	2	−6.45	4,160	70	4,704	Achenes
130054	FWC2D7-41B	2	−6.55	4,490	120	5,145	Charcoal
128497	FWC2D7-43B	2	−6.59	4,510	70	5,163	Charcoal
126712	FWC2D8-5B	2	−6.83	4,340	80	4,914	Achenes
128439	FWC2D8-5E	2	−6.83	4,195	60	4,733	Plant fragment
128440	FWC2D8-5F	2	−6.83	4,145	70	4,689	Plant fragment
130055	SHERCIC3D1-2A	2	−5.48	4,005	70	4,479	Achenes
130056	SHERCIC3D1-12A	2	−5.68	4,225	70	4,751	Achenes
130057	SHERCIC3D2-6A	2	−5.78	4,110	70	4,636	Achenes
130058	SHERCIC3D2-23A	2	−6.12	4,560	70	5,173	Achenes
130059	SHERCIC3D3-2A	2	−6.19	4,590	70	5,311	Achenes
130060	SHERCIC3D3-24A	2	−6.63	5,010	90	5,749	Achenes
130300	SHERCIC3D3-25A	2	−6.65	5,060	70	5,819	Charcoal
130097	SHERCIC3D4-8A	2	−6.81	5,115	80	5,827	Achenes
126713	SHERCIC3D4-15A	2	−6.95	5,425	80	6,237	Achenes
130098	SHERLC2D1-13A	2	−4.95	3,400	80	3,649	Achenes
130099	SHERLC2D2-4A	2	−5.05	3,520	120	3,794	Achenes
130100	SHERLC2D2-34A	2	−5.65	4,160	140	4,689	Charcoal
130101	SHERLC2D3-10B	2	−5.87	3,980	120	4,450	Charcoal
130102	SHERLC2D3-28A	2	−6.23	4,010	200	4,497	Charcoal
130400	SHERLC2D3-28B	2	−6.23	4,280	80	4,850	Granular fragment
130103	SHERLC2D4-24A	2	−7.15	4,950	120	5,687	Charcoal

CAMS lab code	Site, core, and sample ID	Sample thickness (cm)	Sample bottom elevation (MSL in meter)	^{14}C age (^{14}C year BP)	2σ ^{14}C error (^{14}C year BP)	Median probability of 2σ range (cal year BP)	Sample material
130104	SHERLC2D4-46A	2	−7.59	5,530	70	6,331	Achenes
126714	SHERLC2D4-47A	2	−7.61	5,670	70	6,451	Achenes
126724	SHERLC2D4-47B	2	−7.61	5,740	140	6,540	Charcoal
130105	TTC3D1-22A	2	−0.24	60	70	97	Achenes
130106	TTC3D2-45A	2	−1.68	1,265	70	1,214	Achenes
126715	TTC3D5-13A	2	−4.04	2,315	70	2,338	Achenes
130107	VICIC2D1-2A	2	−7.44	3,980	70	4,467	Achenes
130108	VICIC2D2-8A	2	−7.71	4,430	70	5,021	Achenes
130401	VICIC2D2-8B	2	−7.71	4,430	80	5,027	Charcoal
130402	VICIC2D4-8B	2	−8.31	5,400	120	6,202	Granular fragment
130109	VICIC2D4-9A	2	−8.33	5,530	70	6,331	Achenes
130110	VICIC2D4-19A	2	−8.53	5,620	70	6,397	Achenes
130403	VICIC2D4-19B	2	−8.53	5,740	70	6,538	Plant fragment
136901	VIPPC4D3-18A	2	−6.24	4,070	120	4,580	Plant fragment
130404	VICIC2D4-38B	2	−8.91	5,800	160	6,600	Charcoal
126716	VICIC2D4-39A	2	−8.93	5,870	70	6,694	Achenes
130111	VIPPC4D1-8A	2	−5.04	3,085	70	3,307	Charcoal
130112	VIPPC4D4-25A	2	−7.36	4,990	70	5,714	Achenes
130113	VIPPC4D4-49A	2	−7.84	5,300	70	6,083	Achenes
130114	VIPPC4D5-5A	2	−7.96	5,410	90	6,225	Achenes
126717	VIPPC4D5-22A	2	−8.30	5,790	70	6,591	Achenes
126725	VIPPC4D5-23B	2	−8.32	5,610	200	6,406	Charcoal
126726	VIPPC4D5-23C	2	−8.32	5,730	100	6,528	Plant fragment
130115	WTCIC2D1-3A	2	−7.92	4,090	80	4,604	Achenes
130116	WTCIC2D1-7A	2	−7.99	4,355	80	4,925	Achenes
130117	WTCIC2D2-4A	2	−8.08	4,715	70	5,453	Achenes
130118	WTCIC2D2-12A	2	−8.24	4,825	70	5,530	Achenes
130388	WTCIC2D3-4B	2	−8.33	5,075	80	5,817	Charcoal
130389	WTCIC2D3-21A	2	−8.67	5,105	70	5,818	Achenes
130405	WTCIC2D3-21C	2	−8.67	5,330	70	6,107	Charcoal
130390	WTCIC2D4-4A	2	−8.77	5,655	90	6,437	Achenes
130406	WTCIC2D4-4B	2	−8.77	5,385	80	6,203	Charcoal
130391	WTCIC2D4-12A	2	−8.93	5,670	70	6,451	Achenes
130392	WTCIC2D5-2C	2	−9.07	5,820	60	6,634	Achenes
126718	WTCIC2D5-3A	2	−9.09	5,800	70	6,601	Achenes
126727	WTCIC2D5-3B	2	−9.09	5,920	560	6,769	Charcoal
130393	WTLC3D1-10A	2	-6.72	3,825	70	4,223	Charcoal
130394	WTLC3D2-5A	2	−7.09	4,300	60	4,858	Charcoal
130395	WTLC3D3-8A	2	−7.63	4,750	70	5,513	Plant fragment
130396	WTLC3D4-21B	2	−8.20	5,500	80	6,300	Granular fragment
130397	WTLC3D4-35A	2	−8.48	5,765	70	6,567	Achenes
126719	WTLC3D5-8A	2	−8.68	5,830	80	6,643	Achenes
126728	WTLC3D5-8B	2	−8.68	5,905	60	6,722	Charcoal
Shlemon and Begg (1975)	Devils Is., 0.9 m	Unknown	0.9[a]	860	170	809	Bulk peat
Shlemon and Begg (1975)	Devils Is., 2.4 m	Unknown	2.40[a]	2,420	140	2,495	Bulk peat

CAMS lab code	Site, core, and sample ID	Sample thickness (cm)	Sample bottom elevation (MSL in meter)	^{14}C age (^{14}C year BP)	2σ ^{14}C error (^{14}C year BP)	Median probability of 2σ range (cal year BP)	Sample material
Shlemon and Begg (1975)	Devils Is., 4.0 m	Unknown	4.00[a]	3,575	260	3,905	Bulk peat
Shlemon and Begg (1975)	Terminus Is. 6.1 m	Unknown	6.10[a]	3,315	150	3,564	Bulk peat
Shlemon and Begg (1975)	W. Sherman Is. 6.1 m	Unknown	6.10[a]	3,900	140	4,327	Bulk peat
Shlemon and Begg (1975)	Twitchell Is., 6.1 m	Unknown	6.10[a]	3,090	190	3,276	Bulk peat
Shlemon and Begg (1975)	Sherman Is., 9.1 m	Unknown	9.10[a]	4,340	195	4,948	Bulk peat
Shlemon and Begg (1975)	Andrus Is., 9.1 m	Unknown	9.10[a]	4,675	200	5,359	Bulk peat
Shlemon and Begg (1975)	Sherman Is., 12.2 m	Unknown	12.20[a]	6,635	320	7,501	Bulk peat
Shlemon and Begg (1975)	Sherman Is. 15.2 m	Unknown	15.20[a]	6,805	350	7,668	Bulk peat
Atwater et al. (1977)	Borehole 35	Unknown	−7.90	3,360	105	3,608	Salt marsh plant roots
Atwater et al. (1977)	Borehole 25	Unknown	−6.60	3,930	105	4,365	Salt marsh plant fragments
Atwater et al. (1977)	Borehole 36	Unknown	−9.00	5,745	185	6,562	Salt marsh plant roots
Atwater et al. (1977)	Borehole 32	Unknown	−11.40	5,845	100	6,656	Forams and/or diatoms
Atwater et al. (1977)	Borehole 33	Unknown	−10.80	6,200	320	7,053	Forams and/or diatoms
Atwater et al. (1977)	Borehole 21	Unknown	−9.20	6,855	115	7,708	Unknown
Atwater et al. (1977)	Borehole 11	Unknown	−24.60	8,230	135	9,201	Forams and/or diatoms
Atwater et al. (1977)	Borehole 10	Unknown	−21.00	8,295	135	9,270	Forams and/or diatoms
Atwater et al. (1977)	Borehole 16	Unknown	−18.70	8,365	135	9,337	Forams and/or diatoms
Shlemon and Begg (1975)	Devils Is., 9 m	Unknown	0.9[a]	860	170	809	Bulk peat
Shlemon and Begg (1975)	Devils Is., 2.4 m	Unknown	2.40[a]	2,420	140	2,495	Bulk peat
Shlemon and Begg (1975)	Devils Is., 4.0 m	Unknown	4.00[a]	3,575	260	3,905	Bulk peat
Shlemon and Begg (1975)	Terminus Is., 6.1 m	Unknown	6.10[a]	3,315	150	3,564	Bulk peat
Shlemon and Begg (1975)	W. Sherman Is., 6.1 m	Unknown	6.10[a]	3,900	140	4,327	Bulk peat
Shlemon and Begg (1975)	Twitchell Is., 6.1 m	Unknown	6.10[a]	3,090	190	3,276	Bulk peat
Shlemon and Begg (1975)	Sherman Is., 9.1 m	Unknown	9.10[a]	4,340	195	4,948	Bulk peat
Shlemon and Begg (1975)	Andrus Is., 9.1 m	Unknown	9.10[a]	4,675	200	5,359	Bulk peat
Shlemon and Begg (1975)	Sherman Is., 12.2 m	Unknown	12.20[a]	6,635	320	7,501	Bulk peat
Shlemon and Begg (1975)	Sherman Is., 15.2 m	Unknown	15.20[a]	6,805	350	7,668	Bulk peat

In addition, data from Shlemon and Begg (1975) collected in the Delta and data from Atwater et al. (1977) collected in San Francisco Bay are included.

Achenes were all from the genus *Schoenoplectus*, with the majority identified as *S. acutus* var. *occidentalis*. Granular fragments are unidentified organic material that may be fern spores

[a] Represents depths below land surface (m) and not elevation relative to MSL.

References

Allen, J.R.L. 2000. Morphodynamics of Holocene salt marshes: A review sketch from the Atlantic and Southern North Sea coasts of Europe. *Quaternary Science Reviews* 19: 1155–1231.

Anisfield, S.C., M.J. Tobin, and G. Benoit. 1999. Sedimentation rates in flow-restricted and restored salt marshes in Long Island Sound. *Estuaries* 22: 231–244.

Atwater, B.F. 1980. Attempts to correlate late Quaternary climatic records between San Francisco Bay, the Sacramento–San Joaquin Delta, and the Mokelumne River, California. Ph.D. Dissertation. University of Delaware, Newark, DE, USA.

Atwater, B.F. 1982. Geologic maps of the Sacramento–San Joaquin Delta, California. US Geological Survey Miscellaneous Field Studies Map MF-1401, 20 map sheets, scale 1:24,000, Reston, Virginia.

Atwater, B.F. and D.F. Belknap. 1980. Tidal-wetland deposits of the Sacramento–San Joaquin Delta, California. *Pacific Coast Paleogeography Symposium* 4: 89–103.

Atwater, B.F., C.W. Hedel, and E.J. Helley. 1977. Late Quaternary depositional history, Holocene sea-level changes, and vertical crust movement, southern San Francisco Bay, California. US Geological Survey Professional Paper 1014, Washington, DC.

Bartberger, E.C. 1976. Sediment cores and sediment rates, Chincoteague Bay, Maryland and Virginia. *Journal of Sedimentary Petrology* 46: 326–336.

Bloom, A.L. 1964. Peat accumulation and compaction in a Connecticut coastal marsh. *Journal of Sedimentary Petrology* 34: 599–603.

Byrne, R.B., B.L. Ingram, S. Starratt, and F. Malamud-Roam. 2001. Carbon-isotope, diatom, and pollen evidence for late Holocene salinity change in a brackish marsh in the San Francisco Estuary. *Quaternary Research* 55: 66–76.

Cahoon, D.R., P.F. Hensel, T. Spencer, D.J. Reed, K.L. McKee, and N. Saintilan. 2006. Coastal wetland vulnerability to sea-level rise: Wetland elevation trends and process controls. In *Wetlands and natural resource management: Ecological studies Vol. 190*, ed. J.T.A. Verhoeven, B. Beltman, R. Bobbink, and D.F. Whigham, 271–292. Berlin: Springer.

California Department of Water Resources. 1995. Sacramento–San Joaquin Delta Atlas. Central District, Sacramento, California, USA, http://baydeltaoffice.water.ca.gov/DeltaAtlas/index.cfm.

Church, J.A. and N.J. White. 2006. A 20th century acceleration in global sea-level rise. *Geophysical Research Letters* 33: L01602. doi:10.1029/2005GL024826.

Cayan, D.R. and D.H. Peterson. 1993. Spring climate and salinity in the San Francisco Bay estuary. *Water Resources Research* 29: 293–303.

Conomos, T.J. 1979. Properties and circulation of San Francisco Bay waters. In *San Francisco Bay: The urbanized estuary*, ed. T.J. Conomos, 47–84. San Francisco: Pacific Division, American Association for the Advancement of Science.

DeLaune, R.D., R.H. Baumann, and J.G. Gosselink. 1983. Relationships among vertical accretion, coastal submergence, and erosion in a Louisiana Gulf coast marsh. *Journal of Sedimentary Petrology* 53: 147–157.

Deverel, S.J. and S.A. Rojstaczer. 1996. Subsidence of agricultural lands in the Sacramento–San Joaquin Delta, California: Role of aqueous and gaseous carbon fluxes. *Water Resources Research* 32: 2359–2367.

Deverel, S.J., and D.A. Leighton. 2009. Subsidence causes and rates in the Sacramento–San Joaquin Delta and Suisun Marsh. San Francisco Estuary and Water Science, in press.

Deverel, S.J., B. Wang, and S. Rojstaczer. 1998. Subsidence of organic soils, Sacramento–San Joaquin Delta, California. In *Land subsidence case studies and current research, special publication no. 8*, ed. J.W. Borchers, 489–502. Denver: Association of Engineering Geologists.

Drexler, J.Z., C.S. de Fontaine, and D.L. Knifong. 2007. Age determination of the remaining peat in the Sacramento–San Joaquin Delta, California, USA. US Geological Survey Open File Report 2007-1303, Sacramento, California.

Drexler, J.A., C.S. de Fontaine, and S.J. Deverel. 2009. The legacy of wetland drainage on the remaining peat in the Sacramento–San Joaquin Delta, California, USA. *Wetlands* 29: 372–386.

Enzel, Y., D.R. Cayan, R.Y. Anderson, and S.G. Wells. 1989. Atmospheric circulation during Holocene lake stands in the Mojave Desert: Evidence of regional climate change. *Nature* 341: 44–47.

French, J. 2006. Tidal marsh sedimentation and resilience to environmental change: Exploratory modeling of tidal, sea-level, and sediment supply forcing in predominantly allochthonous systems. *Marine Geology* 235: 119–136.

Gilbert, G.K. 1917. *Hydraulic-mining debris in the Sierra Nevada. US Geological Survey professional paper 105*. Washington, DC: US Government Printing Office.

Givelet, N., G. Le Roux, A. Cheburkin, B. Chen, J. Frank, M. Goodsite, H. Kempter, M. Krachler, T. Noernberg, N. Rausch, S. Rheinberger, F. Roos-Barraclough, A. Sapkota, C. Scholz, and W. Shotyk. 2004. Suggested protocol for collecting, handling and preparing peat cores and peat samples for physical, chemical, mineralogical and isotopic analyses. *Journal of Environmental Monitoring* 6: 481–492.

Goman, M. and L. Wells. 2000. Trends in river flow affecting the northeastern reach of the San Francisco Bay Estuary over the past 7000 years. *Quaternary Research* 54: 206–217.

Hatton, R.S., R.D. DeLaune, and W.H. Patrick Jr. 1983. Sedimentation, accretion, and subsidence in marshes of Barataria Basin, Louisiana. *Limnology and Oceanography* 28: 494–502.

Heegaard, E., H.J.B. Birks, and R.J. Telford. 2005. Relationships between calibrated ages and depth in stratigraphical sequences: An estimation procedure by mixed-effect regression. *The Holocene* 15: 612–618.

Heiri, O., A.F. Lotter, and G. Lemcke. 2001. Loss on ignition as a method for estimating organic and carbonate content in sediments; reproducibility and comparability of results. *Journal of Paleolimnology* 25: 101–110.

Hensel, P.F., J.W. Day Jr., and D. Pont. 1998. Wetland vertical accretion and soil elevation change in the Rhone River Delta, France: The importance of riverine flooding. *Journal of Coastal Research* 15: 668–681.

Hickman, J.C. (ed). 1993. *The Jepson manual*. Berkeley: University of California Press.

Hillel, D. 1998. *Environmental soil physics: Fundamentals, applications, and environmental considerations*. San Diego: Elsevier Science and Technology.

Ingebritsen, S.E. and M.E. Ikehara. 1999. Sacramento–San Joaquin Delta: The sinking heart of the state. In *Land subsidence in the United States*, ed. D. Galloway, D.R. Jones, and S.E. Ingebritsen, 83–94. Reston: US Geological Survey. Circular 1182.

Kaye, C.A. and E.S. Barghoorn. 1964. Late Quaternary sea level and crustal rise at Boston, Massachusetts with notes on the autocompaction of peat. *Geological Society of America Bulletin* 75: 63–80.

Keene, H.W. 1971. Postglacial submergence and salt marsh evolution in New Hampshire. *Maritime Sediments* 7: 64–68.

Khan, H. and G.S. Brush. 1994. Nutrient and metal accumulation in a freshwater tidal marsh. *Estuaries* 17: 345–360.

LaMarche Jr., V. 1973. Holocene climatic variations inferred from tree line fluctuations in the White Mountains California. *Quaternary Research* 3: 632–660.

Liu, K.B., S. Sun, and X. Jiang. 1992. Environmental change in the Yangtze River delta since 12,000 years BP. *Quaternary Research* 38: 32–45.

McKensie, N., K. Coughlan, and H. Cresswell. 2002. *Soil physical measurement and interpretation for land evaluation*. Australian Collaborative Land Evaluation Program, Natural Heritage Trust, CSIRO Publishing.

Meehl, G.A., T.F. Stocker, W.D. Collins, P. Friedlingstein, A.T. Gaye, J.M. Gregory, A. Kitoh, R. Knutti, J.M. Murphy, A. Noda, S.C. B. Raper, I.G. Watterson, A.J. Weaver, and Z.-C. Zhao. 2007. Global climate projections. In *Climate change 2007: The physical science basis. Contribution of working group I to the fourth assessment report of the Intergovernmental Panel on Climate Change*, ed. S.D. Solomon, D. Qin, M. Manning, Z. Chen, M. Marquis, K.B. Avery, M. Tignor, and H.L. Miller, 749–845. Cambridge: Cambridge University Press.

Merrill, J.Z. and J.C. Cornwell. 2000. The role of oligohaline marshes in estuarine nutrient cycling. In *Concepts and controversies in tidal marsh ecology*, ed. M. Weinstein and D.A. Kreeger, 425–441. Dordrecht: Kluwer.

Miller Jr., R.G. 1998. *Beyond ANOVA: Basic of applied statistics*. Boca Raton: CRC.

Miller, R.L., L. Hastings, and R. Fujii. 1997. Hydrologic treatments affect gaseous carbon loss from organic soils, Twitchell Islands, California, October 1995–December 1997. US Geological Survey Water-Resources Investigations Report 00-4042, Sacramento, California.

Mitsch, W.J. and J.G. Gosselink. 2000. *Wetlands*, 3rd ed. New York: Wiley.

Mount, J. and R. Twiss. 2005. Subsidence, sea level rise, seismicity in the Sacramento–San Joaquin Delta. *San Francisco Estuary and Watershed Science* 3(1): Article 5. http://repositories.cdlib.org/jmie/sfews/vol3/iss1/art5.

Neubauer, S.C. 2008. Contributions of mineral and organic components to tidal freshwater marsh accretion. *Estuarine, Coastal and Shelf Science* 78: 78–88.

Okruszko, H. 1971. Determination of specific gravity of hydrogenic soils on the basis of their mineral particles content. *Wiadomosci Instytutu Melioracji i Uzytkow Zielonych* X(1): 47–54.

Orr, M., S. Crooks, and P.B. Williams. 2003. Will restored tidal marshes be sustainable? *San Francisco Estuary and Watershed Science* 1(1): Article 5. http://respositories.cdlib.org/jmie/sfews/vol1/iss1/art5.

Orson, R.A., R.L. Simpson, and R.E. Good. 1990. Rates of sediment accumulation in a tidal freshwater marsh. *Journal of Sedimentary Petrology* 60: 859–869.

Penland, S. and K.E. Ramsey. 1990. Relative sea-level rise in Louisiana and the Gulf of Mexico: 1908–1988. *Journal of Coastal Research* 6: 323–342.

Pizzuto, J.E. and A.E. Schwendt. 1997. Mathematical modeling of autocompaction of a Holocene transgressive valley-fill deposit, Wolfe Glade, Delaware. *Geology* 25: 57–60.

Prokopovich, N.P. 1985. Subsidence of peat in California and Florida. *Bulletin of the Association of Engineering Geologists* 22: 395–420.

Redding, T.E. and K.J. Devito. 2006. Particle densities of wetland soils in northern Alberta, Canada. *Canadian Journal of Soil Science* 86: 57–60.

Redfield, A.C. 1967. Postglacial change in sea level in the western north Atlantic Ocean. *Science* 157: 687–690.

Reed, D.J. 2000. Coastal biogeomorphology: An integrated approach to understanding the evolution, morphology, and sustainability of temperate coastal marshes. In *Estuarine science: A synthetic approach to research and practice*, ed. J.E. Hobbie, 347–361. Washington, DC: Island Press.

Reed, D.J. 2002a. Sea-level rise and coastal marsh sustainability: geological and ecological factors in the Mississippi delta plain. *Geomorphology* 48: 233–243.

Reed, D.J. 2002b. Understanding tidal marsh sedimentation in the Sacramento–San Joaquin Delta, California. *Journal of Coastal Research SI* 36: 605–611.

Reimer, P.J., M.G.L. Baillie, E. Bard, A. Bayliss, J.W. Beck, C.J.H. Bertrand, P.G. Blackwell, C.E. Buck, G.S. Burr, K.B. Cutler, P.E. Damon, R.L. Edwards, R.G. Fairbanks, M. Friedrich, T.P. Guilderson, A.G. Hogg, K.A. Hughen, B. Kromer, G. McCormac, S. Manning, C.B. Ramsey, R.W. Reimer, S. Remmele, J.R. Southon, M. Stuiver, S. Talamo, F.W. Taylor, J. van der Plicht, and C.E. Weyhenmeyer. 2004. IntCal04 terrestrial radiocarbon age calibration, 0–26 cal kyr BP. *Radiocarbon* 46: 1029–1058.

Robinson, S.D. and T.R. Moore. 1999. Carbon and peat accumulation over the past 1200 years in a landscape with discontinuous permafrost, northwestern Canada. *Global Biogeochemical Cycles* 13: 591–601.

Rojstaczer, S. and S.J. Deverel. 1993. Time dependence in atmospheric carbon inputs from drainage of organic soils. *Geophysical Research Letters* 20: 1383–1386.

Rojstaczer, S. and S.J. Deverel. 1995. Land subsidence in drained histosols and highly organic mineral soils of California. *Soil Science Society of America Journal* 59: 1162–1167.

Rojstaczer, S.A., R.E. Hamon, S.J. Deverel, and C.A. Massey. 1991. Evaluation of selected data to assess the causes of subsidence in the Sacramento-San Joaquin Delta, California. Open-File Report 91-0193, US Geological Survey, Reston, Virginia.

Roman, C.T., J.A. Peck, J.R. Allen, J.W. King, and P.G. Appleby. 1997. Accretion of a New England (USA) salt marsh in response to inlet migration, storms, and sea-level rise. *Estuarine, Coastal and Shelf Science* 45: 717–727.

Sawai, Y., N. Hiroo, and Y. Yasuda. 2002. Fluctuations in relative sea-level during the past 3000 yr in the Onnetoh estuary, Hokkaido, northern Japan. *Journal of Quaternary Science* 17: 607–622.

Schoellhamer, D., S. Wright, J.Z. Drexler, M. Stacey, and S.C. Model. 2007. *White paper for the California Bay/Delta Science Program*. Sacramento: The Resources Agency of the State of California.

Service, R.J. 2007. Delta blues, California style. *Science* 317: 442–445.

Shennan, I., A.J. Long, M.M. Rutherford, J.B. Innes, F.M. Green, J.R. Kirby, and K.J. Walker. 1998. Tidal marsh stratigraphy, sea-level change and large earthquake—II: Submergence events during the last 3500 years at Netarts Bay, Oregon, USA. *Quaternary Science Reviews* 17: 365–393.

Shlemon, R.J. and E.L. Begg. 1975. Late quaternary evolution of the Sacramento–San Joaquin Delta, California. In *Quaternary studies*, ed. R.P. Suggate and M.M. Creswell, 259–266. Wellington: The Royal Society of New Zealand.

Stanley, D.J. and A.G. Warne. 1994. Worldwide initiation of Holocene marine deltas by deceleration of sea-level rise. *Science* 265: 228–231.

Stevenson, J.C., M.S. Kearney, and E.C. Pendleton. 1986. Vertical accretion rates in marshes with varying rates of sea-level rise. In *Estuarine variability*, ed. D. Wolfe, 241–260. New York: Academic.

Stine, S. 1990. Late Holocene fluctuations of Mono Lake, eastern California. *Palaeogeography, Palaeoclimatology, Palaeoecology* 78: 333–381.

Stuiver, M. and P.J. Reimer. 1993. Extended ^{14}C data base and revised CALIB 3.0 ^{14}C age calibration program. *Radiocarbon* 35: 215–230.

Temmerman, S., G. Govers, S. Wartel, and P. Meire. 2003. Spatial and temporal factors controlling short-term sedimentation in a salt and freshwater tidal marsh, Scheldt estuary, Belgium, SW Netherlands. *Earth Surface Processes and Landforms* 28: 739–755.

Thompson, J. 1957. The settlement geography of the Sacramento–San Joaquin Delta, California. Ph.D. Dissertation. Stanford University, Stanford, California, USA.

Tornqvist, T.E., A.F.M. De Jong, W.A. Oosterbaan, and K. Van der Borg. 1992. Accurate dating or organic deposits by AMS ^{14}C measurement of macrofossils. *Radiocarbon* 34: 566–577.

Tornqvist, T.E., J.L. Gonzalez, L.E. Newsom, K. van der Borg, A.F.M. de Jong, and C.W. Kurnik. 2004. Deciphering Holocene sea-level history on the US Gulf Coast: A high-resolution record from the Mississippi Delta. *GSA Bulletin* 116: 1026–1039.

Tornqvist, T.E., S.J. Bick, K. van der Borg, and A.F.M. de Jong. 2006. How stable is the Mississippi Delta? *Geology* 34: 697–700.

Turetsky, M.R., S.W. Manning, and R.K. Wieder. 2004. Dating recent peat deposits. *Wetlands* 24: 324–356.

United States Department of Agriculture Soil Conservation Service. 2006. Keys to soil taxonomy. 10th edition. ftp://ftp-fc.sc.egov.usda.gov/NSSC/Soil_Taxonomy/keys/keys.pdf.

van Heteren, S. and O. van de Plassche. 1997. Influence of relative sea-level change and tidal inlet development on barrier-spit stratigraphy, Sandy Neck, Massachusetts. *Journal of Sedimentary Research* 67: 350–363.

Weber-Band, J. 1998. Neotectonics of the Sacramento-San Joaquin Delta area, east central Coast Ranges, California. Ph.D. thesis, University of California, Berkeley, California, USA.

Wells, L.E. 1995. Radiocarbon dating of Holocene tidal marsh deposits: Applications to reconstructing relative sea level changes in the San Francisco estuary. In *Quaternary geochronology and paleoseismology*, ed. J.S. Noller, W.R. Lettis, and J.M. Sowers, 3.95–3.102. Washington DC: Nuclear Regulatory Commission.

Witter, R.C., H.M. Kelsey, and E. Hemphill-Haley. 2003. Great Cascadia earthquakes and tsunamis of the past 6700 years, Coquille River estuary, southern coastal Oregon. *Geological Society of America Bulletin* 115: 1289–1306.

Wright Jr., H.E. 1991. Coring tips. *Journal of Paleolimnology* 6: 37–49.

Wright, S.A. and D.H. Schoellhamer. 2004. Trends in the sediment yield of the Sacramento River, California, 1957–2001. *San Francisco Estuary and Watershed Science* 2(2): Article 2. http://repositories.cdlib.org/jmie/sfews/vol2/iss2/art2.

Wright, S.A. and D.H. Schoellhamer. 2005. Estimating sediment budgets at the interface between rivers and estuaries with application to the Sacramento–San Joaquin River Delta. *Water Resources Research* 41: W09428. doi:10.1029/2004WR003753.

Yang, S.L., I.M. Belkin, A.I. Belina, Q.Y. Zhao, J. Zhu, and P.X. Ding. 2003. Delta response to decline in sediment supply from the Yangtze River: Evidence of the recent four decades and expectations for the next half-century. *Estuarine, Coastal and Shelf Science* 57: 689–699.

Zoltai, S.C. and J.D. Johnson. 1984. Development of a treed bog island in a minerotrophic fen. *Canadian Journal of Botany* 63: 1076–1085.